

Rochester Institute of Technology

**RIT Digital Institutional Repository**

---

Theses

---

9-2019

## **Rotor Current Control Design for DFIG-based Wind Turbine Using PI, FLC and Fuzzy PI Controllers**

Omar Al-Zabin  
osa8662@rit.edu

Follow this and additional works at: <https://repository.rit.edu/theses>

---

### **Recommended Citation**

Al-Zabin, Omar, "Rotor Current Control Design for DFIG-based Wind Turbine Using PI, FLC and Fuzzy PI Controllers" (2019). Thesis. Rochester Institute of Technology. Accessed from

This Thesis is brought to you for free and open access by the RIT Libraries. For more information, please contact [repository@rit.edu](mailto:repository@rit.edu).

---

# **Rotor Current Control Design for DFIG-based Wind Turbine Using PI, FLC and Fuzzy PI Controllers**

By

Omar Al Zabin Al-Khaldi

A Thesis Submitted in Partial Fulfilment of the Requirements for the Degree of Master  
of Science in Electrical Engineering Department of Electrical Engineering and  
Computing Sciences.

**Department of Electrical Engineering and Computing Sciences**

Rochester Institute of Technology - Dubai

September 2019

---

---

# **Rotor Current Control Design for DFIG-based Wind Turbine Using PI, FLC and Fuzzy PI Controllers**

By

Omar Al Zabin Al-Khaldi

A Thesis Submitted in Partial Fulfilment of the Requirements  
for the Degree of Master of Science in Electrical Engineering  
Department of Electrical Engineering and Computing Sciences

**Approved By:**

**Date:**

---

Dr. Abdulla Ismail

*Thesis advisor*

*Professor of Electrical Engineering and Computer Science,*

*RIT Dubai*

**Date:**

---

Dr. Mohamed Samaha,

*Associate Professor of Mechanical Engineering,*

*RIT Dubai*

**Date:**

---

Dr. Jinane Mounsef

*Assistant Professor of Electrical and Computer Science,*

*RIT Dubai*

---

# Acknowledgement

I would like to thank my supervisor Dr. Abdulla Ismail for his assistance and guidance.

My greatest thanks to my manager and elder brother, Engineer Samer Amin Al Mahdawi, for his unlimited support and cooperation. Without your help and wide span of knowledge, my success would have been difficult.

I would like to appreciate and thank my mother for her encouragement and support that motivated me to start and complete my MSc journey. I would also like to thank my family for their unfailing love, support, and patience.

Sincere appreciation is extended to my wife, for her unconditional encouragement, unlimited love and infinite enthusiasm; I could not have gone through this journey without your help and support.

*To my beloved daughter and son*

# Abstract

Due to the rising demand for electricity with increasing world population, maximizing renewable energy capture through efficient control systems is gaining attention in literature. Wind energy, in particular, is considered the world's fastest growing energy source it is one of the most efficient, reliable and affordable renewable energy sources. Subsequently, well-designed control systems are required to maximize the benefits, represented by power capture, of wind turbines.

In this thesis, a 2.0-MW Doubly-Fed Induction Generator (DFIG) wind turbine is presented along with new controllers designed to maximize the wind power capturer. The proposed designs mainly focus on controlling the DFIG rotor current in order to allow the system to operate at a certain current value that maximizes the energy capture at different wind speeds. The simulated model consists of a single two-mass wind turbine connected directly to the power grid. A general model consisting of aerodynamic, mechanical, electrical, and control systems are simulated using Matlab/Simulink. An indirect speed controller is designed to force the aerodynamic torque to follow the maximum power curve in response to wind variations, while a vector controller for current loops is designed to control the rotor side converter.

The control system design techniques considered in this work are Proportional-Integral (PI), fuzzy logic, and fuzzy-PI controllers. The obtained results show that the fuzzy-PI controller meets the required specifications by exhibiting the best steady state response, in terms of steady state error and settling time, for some DFIG parameters such as rotor speed, rotor currents and electromagnetic torque. Although the fuzzy logic controller exhibits smaller peak overshoot and undershoot values when compared to the fuzzy-PI, the peak value difference is very small, which can be compensated using protection equipment such as circuit breakers and resistor banks. On the other hand, the PI controller shows the highest overshoot, undershoot and settling time values, while the fuzzy logic controller does not meet the requirements as it exhibits large, steady-state error values.

# Table of Contents

|  |    |
|--|----|
| Chapter 1 : Introduction .....                   | 10 |
| 1.1 Research Motivation .....                    | 10 |
| 1.2 Problem Statement and Challenges .....       | 11 |
| 1.3 Main Contributions .....                     | 12 |
| 1.4 Thesis Organization.....                     | 13 |
| 1.5 Publications .....                           | 13 |
| Chapter 2 : Overview and Background.....         | 14 |
| 2.1 The Wind.....                                | 14 |
| 2.1.1 The Mean Wind Speed.....                   | 14 |
| 2.1.2 The Energy and Power in the Wind.....      | 16 |
| 2.1.3 The Turbulence .....                       | 17 |
| 2.2 The Wind Turbine .....                       | 17 |
| 2.2.1 Wind Turbine Rotor Design.....             | 17 |
| 2.2.2 Wind Turbine Aerodynamics.....             | 20 |
| 2.2.3 Force, Torque and Power .....              | 20 |
| 2.3 Power Capture by Wind Turbines .....         | 22 |
| 2.4 The Impact of Wind Turbines on the Grid..... | 22 |
| 2.4.1 Location .....                             | 23 |
| 2.4.2 Generators .....                           | 23 |
| 2.6 Literature Review .....                      | 26 |
| Chapter 3 : Modeling Wind Turbines .....         | 29 |
| 3.1 Wind Speed Model.....                        | 30 |
| 3.2 Aerodynamic Model.....                       | 32 |
| 3.3 Mechanical Model.....                        | 33 |

|  |  |    |
|--|--|----|
| 3.4  | Electrical Model .....   | 34 |
| Chapter 4 : Control System Design .....      |  | 37 |
| 4.1  | Introduction .....   | 37 |
| 4.1.1  | Indirect speed control.....  | 37 |
| 4.1.2  | Rotor side converter control.....  | 38 |
| 4.2  | Proportional-Integral Control.....   | 40 |
| 4.3  | Fuzzy Control.....   | 42 |
| 4.4  | Fuzzy PI Control .....   | 45 |
| Chapter 5 : Simulation and Results.....      |  | 47 |
| 5.1  | Model Simulation.....  | 47 |
| 5.1.1  | Wind Speed Model Simulation.....   | 47 |
| 5.1.2  | Aerodynamic Model Simulation.....  | 47 |
| 5.1.3  | Electrical Model Simulation .....  | 48 |
| 5.1.4  | Control System Simulation.....   | 48 |
| 5.2  | Steady state analysis.....   | 50 |
| 5.3  | Performance analysis.....  | 52 |
| 5.3.1  | Simulation results for different wind speeds using PI controller.....        | 52 |
| 5.3.2  | Simulation results for different wind speeds using Fuzzy controller .....    | 56 |
| 5.3.3  | Comparison between Fuzzy Controller and PI controller.....                   | 58 |
| 5.3.4  | Simulation results for different wind speeds using fuzzy-PI controller ..... | 59 |
| 5.3.5  | Comparison between the three proposed controllers .....                      | 61 |
| Chapter 6 : Conclusion and Future Work ..... |  | 64 |
| References.....                              |  | 66 |
| Appendix - I.....                            |  | 70 |



## List of Figures

|   |    |
|---|----|
| Figure 1.1: Total installed capacity of wind power generation 2013-2017 [6].  | 10 |
| Figure 1.2: Annual global fossil fuels carbon emission [7].   | 11 |
| Figure 2.1: Weibull probability distribution of mean wind speeds [1].   | 15 |
| Figure 2.2: Power density VS wind speed [1].  | 15 |
| Figure 2.3: Wind turbine diagram.   | 18 |
| Figure 2.4: (a) Vertical-axis and (b) horizontal-axis wind turbines [1].  | 18 |
| Figure 2.5: Variable speed wind turbine generators; (a) with synchronous generator, (b) with doubly fed induction generator (DFIG) [22].                | 19 |
| Figure 2.6: Fixed speed wind turbine generator [22].  | 19 |
| Figure 2.7: Typical variations of $C_Q$ and $C_P$ for a fixed-pitch wind turbine [1].   | 21 |
| Figure 2.8: (a) Aerodynamic Torque and (b) Power VS rotor speed with wind speed as a parameter and $\beta = 0$ [1].                                     | 21 |
| Figure 3.1: General structure of the wind turbine model. [39]   | 29 |
| Figure 3.2: Mitsubishi MWT 92 wind turbine [43].  | 33 |
| Figure 3.3: Two mass drive train model [41].  | 34 |
| Figure 3.4: DFIM with back to back converter [42].  | 35 |
| Figure 3.5: Control supply configuration for DFIM [42].   | 36 |
| Figure 4.1: Maximum power efficiency curve [43].  | 37 |
| Figure 4.2: Different reference frames that represent space vectors of DFIG [42].   | 39 |
| Figure 4.3: Second-order system of closed-loop current control with PI controllers [42].  | 40 |
| Figure 4.4: (a) the power coefficient ( $C_p$ ) VS the tip speed ratio, (b) the generated power Vs. the wind speed for the 2 MW Mitsubishi design [43]. | 41 |
| Figure 4.5: A triangular membership function  | 42 |
| Figure 4.6: The three phases of the fuzzy logic controller.   | 43 |
| Figure 4.7: Input membership functions for fuzzy controller.  | 44 |
| Figure 4.8: Output membership functions for fuzzy controller.   | 44 |
| Figure 4.9: Input membership functions for fuzzy-PI controller.   | 46 |
| Figure 4.10: Output membership functions for fuzzy-PI controller.   | 46 |
| Figure 5.1: Wind speed model simulation with average speed of 8m/s.   | 47 |

|  |    |
|--|----|
| Figure 5.2: Aerodynamic system simulation of a WT.....   | 48 |
| Figure 5.3: Electrical system simulation of a DFIG wind turbine.....   | 48 |
| Figure 5.4: Control system simulation of a DFIG WT.....  | 49 |
| Figure 5.5: Overall WT dynamic model design in Simulink.....   | 49 |
| Figure 5.6: Steady state magnitudes of a 2 MW DFIG.....  | 52 |
| Figure 5.7: Steady state response of the simulated system with rotor speed of 142.8 rad/sec. ....  | 53 |
| Figure 5.8: PI controller design of the DFIG wind turbine.....   | 53 |
| Figure 5.9: Wind speed signal .....  | 55 |
| Figure 5.10: Steady state simulation for DFIG with PI controller at average wind speed component of 8 m/s.....   | 56 |
| Figure 5.11:Fuzzy logic controller for the rotor current components.....   | 57 |
| Figure 5.12: Steady state simulation for DFIG with fuzzy logic controller at average wind speed component of 8 m/s.....  | 57 |
| Figure 5.13: Steady state simulation for DFIG with fuzzy logic controller and PI controller at average wind speed component of 8 m/s.....                        | 59 |
| Figure 5.14: Fuzzy-PI controller design for rotor current components. ....   | 59 |
| Figure 5.15: Steady state simulation for DFIG with fuzzy-PI controller at average wind speed component of 8 m/s.....   | 61 |
| Figure 5.16: Steady state simulation for DFIG with PI controller, fuzzy logic controller, and fuzzy- PI controller at average wind speed component of 8 m/s..... | 62 |
| Figure 5.17: Extracted power using proposed control schemes with respect to different wind speed values. ....  | 63 |
| Figure 5.18: Extracted power by DFIG using PI, FLC and Fuzzy PI schemes at $v_{aw}= 11$ m/s.....   | 63 |

## List of Tables

|   |    |
|---|----|
| Table 2.1: Typical values of roughness length $z_o$ and roughness exponent $\alpha$ for several types of surfaces [10,12].  | 16 |
| Table 2.2: Summary of different problems related to the power quality [23].   | 26 |
| Table 3.1: Values of $Z_o$ for different types of landscapes. [41]  | 31 |
| Table 4.1: Wind speed values with their corresponding generated power values.   | 41 |
| Table 4.2: Fuzzy rules for fuzzy logic controller.  | 43 |
| Table 4.3: Fuzzy rules for Fuzzy-PI controller.   | 45 |
| Table 5.1: 2 MW DFIG characteristics.   | 50 |
| Table 5.2: Equations of steady state magnitudes when $i_{dr}=0$ [42].   | 51 |
| Table 5.3: Design simulation with certain wind speed values and their corresponding power and steady state magnitudes of the rotor speed and the electromagnetic torque using PI controller.          | 54 |
| Table 5.4: Steady state analysis for DFIG wind turbine with PI controller.  | 56 |
| Table 5.5: Design simulation with certain wind speed values and their corresponding power and steady state magnitudes of the rotor speed and the electromagnetic torque using fuzzy logic controller. | 58 |
| Table 5.6: Steady state analysis for DFIG wind turbine with fuzzy logic controller.   | 58 |
| Table 5.7: Design simulation with certain wind speed values and their corresponding power and steady state magnitudes of the rotor speed and the electromagnetic torque using fuzzy-PI controller.    | 60 |
| Table 5.8: Steady state analysis for DFIG wind turbine with fuzzy-PI controller.  | 61 |

# Chapter 1 : Introduction

This chapter discusses the motivation behind the research presented in this thesis along with a general background of the research topic.

## 1.1 Research Motivation

Since the beginning of human civilization, wind power has been extensively used for water pumping, milling grain and sailing ships [1-5]. However, after the Industrial Revolution at the end of the 18<sup>th</sup> century, the natural resources were heavily replaced by fossil fuels. Yet, during the last decades, particularly after the oil price boost and the wide-spread awareness about healthy environments, wind energy captured researchers' attention and consequently took pride of place in power generation [1-5]. The concerns about the increasing emission of carbon dioxide, which threatens the existence of life this planet, motivated several R&D programs in various countries. These programs were conducted to contribute in developing modern turbine designs that resulted in the evolution of the large-scale wind electricity generation [5]. Nowadays, wind energy is considered the fastest-growing renewable resource worldwide. According to World Wind Energy Association [6], the total capacity of all wind turbines installed worldwide experienced an increase by a factor of 1.8 in the last five years. Fig. 1.1 illustrates the overall installed capacity of wind power generation in the years between 2013 and 2017. All wind turbines, which reached a capacity of 539,291 Megawatt, installed by end of 2017 can cover more than 5% of the global electricity demand. Moreover, Denmark was recognized as one of the leading

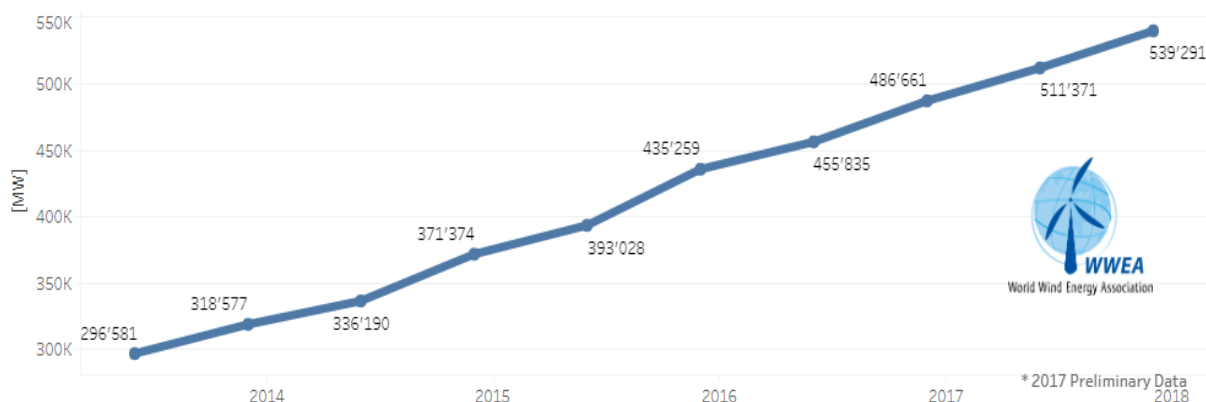


Figure 1.1: Total installed capacity of wind power generation 2013-2017 [6].

countries in the field of wind electricity generation. Forty-three per cent of its generated power depends on wind sources [6]. Moreover, many countries are adopting wind power to generate electricity due to its clean and positive impact on the environment. Wind is considered an endless-supply of renewable energy that generates electricity with very little or no pollution. On the other hand, the fossil fuels, such as coal, oil and natural gas, damage the environment by emitting carbon dioxide when burned. Fig. 1.2 shows the increasing amount of the global carbon emission that results in higher global warming [7]. Cost wise, the price of electricity generated by wind turbines constitutes to a massive drop since the 1980s due to the increasing installed capacity and production scales of wind facilities [1].

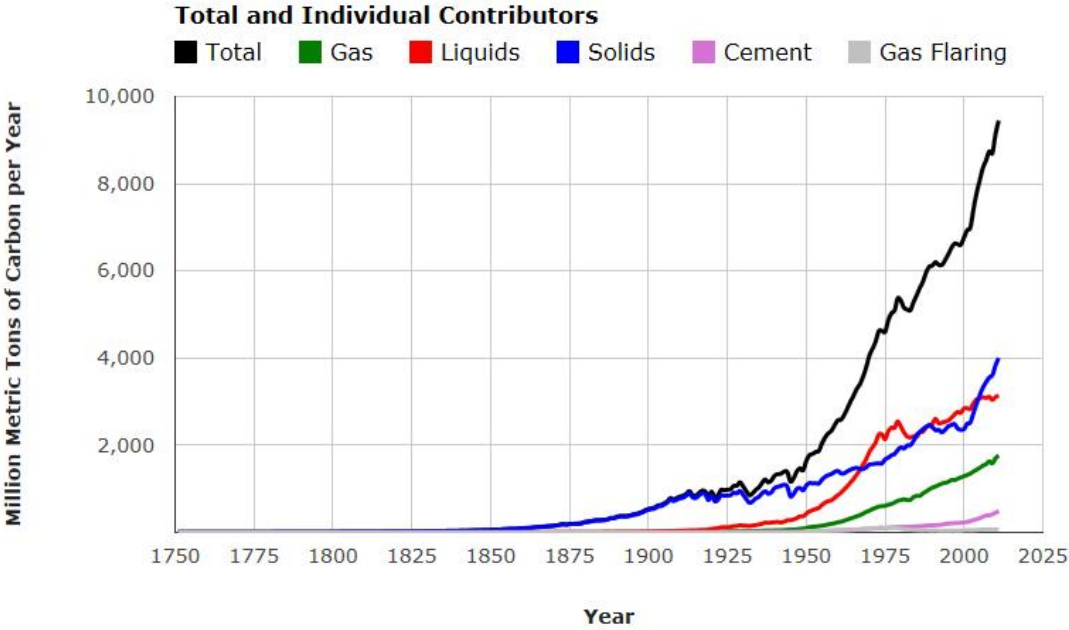


Figure 1.2: Annual global fossil fuels carbon emission [7].

## 1.2 Problem Statement and Challenges

Wind turbine technology has significantly improved in the past few years, resulting in turbines that generate energy at less cost. Nowadays, researchers are competing to enhance the power efficiency of wind turbines in order to get the maximum possible generated electricity supply. However, power efficiency maximization is considered a challenging topic, as there are many factors that play a role in energy capture, such as the surrounding environment, turbine generator design, and control systems [1, 8]. Utilizing efficient control systems in wind turbine design can contribute largely in enhancing wind

power capture, and hence power extraction efficiency. Nevertheless, according to Betz theory, a 100% efficiency cannot be achieved [9]. Betz theory introduces the Betz limit, which is considered as the theoretical upper bound on the maximum extractable power fraction that has the value of  $16/27$ . In other words, a maximum of 59% of the wind power can be extracted using conventional wind turbines. Theoretically speaking, a 100% efficiency cannot be achieved due to the continuous flow of air that has a fluid mechanical nature [1, 9]. As a brief explanation, if 100% of the wind kinetic energy was converted, a complete stop of the wind will occur, and hence, there will not be any further energy extraction by the wind turbine.

Reliable and high performance controllers are required to be designed in such systems to maintain stability and improve efficiency. Different DFIG-based wind turbine control strategies have been widely studied in the literature; such as control of pitch angle, voltage, current, torque, active and reactive power. The advantages of rotor connected back to back voltage source converter control, including reduced flicker, variable speed constant frequency (VSCF) operation, independent control capabilities for active and reactive powers, and relatively lower converter cost and power losses, have captured researchers' and manufacturers attention all over the world [8].

### **1.3 Main Contributions**

The principle contributions of the thesis are:

- Design and simulate DFIG-based wind turbine controller, which meets the required specifications, using Matlab-Simulink. This controller is first designed using a standard conventional PI regulator. The system is then enhanced by following two phases:
  - Replace the conventional PI controller by a Fuzzy Controller to enhance the overshoot/undershoot, oscillations and settling time of the extracted power and DFIG rotor current components.
  - Design a Fuzzy-PI controller to minimize the steady state error along with minimizing overshoot/undershoot, oscillations and settling time of the extracted power and DFIG rotor current components.

## 1.4 Thesis Organization

The thesis is organized as follows:

Chapter 1 discusses the importance of utilizing wind to generate electric power. It also provides an overview of the main challenges and constraints of wind energy capture. Then, the research objectives and contributions are highlighted. The chapter is concluded with a description of the thesis chapters. Chapter 2 highlights the main properties of the wind along with its structures that are crucial for wind turbine controller design. Then a brief description of wind turbine technology is introduced with focus on energy conversion. A literature review is also provided. Chapter 3 discusses and analyzes the modeling of a DFIG wind turbine that consists of wind model, aerodynamic model, mechanical model, and electrical model. Chapter 4 introduces the designed DFIG wind turbine controls: PI, Fuzzy logic control and Fuzzy-PI control. The results and comparisons are discussed. Chapter 5 concludes the thesis with suggestions for future work.

## 1.5 Publications

- O. Al Zabin and A. Ismail, “Rotor current controller design for DFIG-based wind turbine using PI, FLC and Fuzzy PI controllers,” *To be presented in IEEE International Conference on Electrical and Computing Technologies and Applications (ICECTA)*, UAE, Nov, 2019.

# Chapter 2 : Overview and Background

This chapter describes the main properties of the wind along with its structures that are crucial for wind turbine controllers design. Then a brief description of wind turbine technology is introduced with focus on energy conversion.

## 2.1 The Wind

The wind is defined as the flow of air masses in the atmosphere as a result of temperature differences. Usually, the geostrophic and local winds are combined to create the wind near the surface of the earth. Hence, the wind used in power generation mainly depends on the geographical areas, the weather, the height above ground level, and the roughness of the surface and surroundings [1, 9]. The main wind properties such as the mean wind speed, the energy in the wind, and the turbulence are discussed in this section.

### 2.1.1 The Mean Wind Speed

The quasi-steady mean wind speed is considered as one of the most important properties of the wind due to its role in determining the commercial feasibility of a wind energy project [1]. This property is crucial to select Wind Energy Conversion Systems (WECS) to maximize the efficiency and firmness. Wind speed measurements and records are collected for several years to predict the probability distribution of the mean wind speed. All this information is usually exhibited in a histogram. The wind distribution can be approximated by a Weibull distribution which is given by [1]:

$$p(V_m) = \frac{k}{c} \left(\frac{V_m}{c}\right)^{k-1} e^{-\left(\frac{V_m}{c}\right)^k}, \quad (2.1)$$

where  $k$  and  $C$  are the shape and scale coefficients respectively, and  $V_m$  is the wind instantaneous speed. These coefficients are adjusted to match the wind data at a particular site [10].



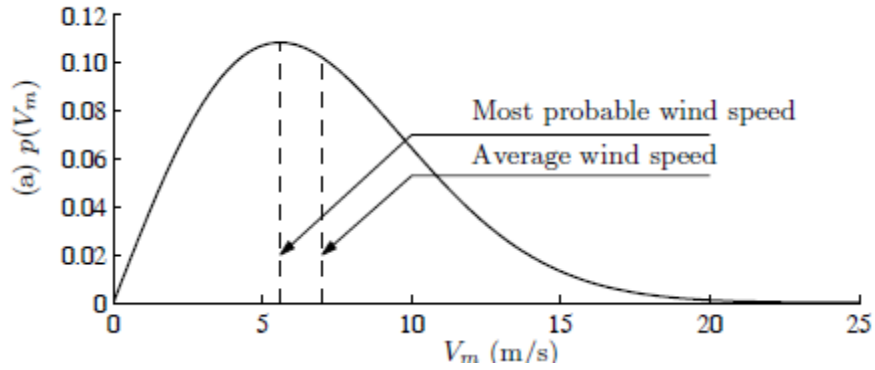


Figure 2.1: Weibull probability distribution of mean wind speeds [1].

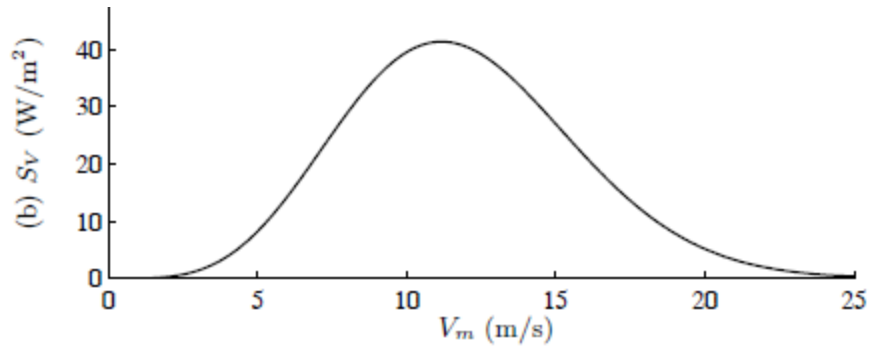


Figure 2.2: Power density VS wind speed [1].

The Weibull probability function shows that winds with high speed rarely occur, whereas winds are more frequent. As shown in Fig. 2.1, the most probable mean wind speed is approximately 5.5 m/s while the average wind speed is approximately 7 m/s. The mean wind speed is also affected by the height of the wind. The friction of low wind layers with the ground surface generates a force opposite to the wind direction which is called wind shear. In literature, several mathematical models have been addressed to study the wind shear. One of these models is the Prandtl logarithmic law [11]

$$\frac{V_m(z)}{V_m(z_{ref})} = \frac{\ln(\frac{z}{z_0})}{\ln(\frac{z_{ref}}{z_0})}, \quad (2.2)$$

where  $z$  is the vertical height from ground level,  $z_{ref}$  is the reference height (usually 10 m), and  $z_0$  is the roughness length. The roughness length has different values based on the type of the surface as listed in Table 2.1. Another formula that is usually used to describe the effect of the terrain on the wind speed gradient is presented in Eq. (2.3) [12],

$$V_m(z) = V_m(z_{ref}) \left( \frac{z}{z_{ref}} \right)^\alpha, \quad (2.3)$$

where the ground surface roughness exponent  $\alpha$  is also a terrain-dependent parameter that has different values depending on the surface type as shown in the last column of Table 2.1.

Table 2.1: Typical values of roughness length  $z_o$  and roughness exponent  $\alpha$  for several types of surfaces [10,12].

| Type of surface | $z_o$ (mm)   | $\alpha$ |
|-----------------|--------------|----------|
| Sand            | 0.2 to 0.3   | 0.10     |
| Mown grass      | 1 to 10      | 0.13     |
| High grass      | 40 to 100    | 0.19     |
| suburb          | 1000 to 2000 | 0.32     |

### 2.1.2 The Energy and Power in the Wind

In order to tell how much kinetic energy is captured by the wind turbine, it is essential to first study the total energy in the wind. The wind kinetic energy is defined as the amount of energy stored in an airflow due to its motion. The kinetic energy per unit volume can be described by the following equation [1,9]:

$$E_k = \frac{1}{2} \rho v^2, \quad (2.4)$$

where  $\rho$  is the air density and  $v$  is the air speed. It is also important to distinguish between the energy and the power terms. Power is defined as the time rate of energy [9]. Hence, for an air flowing through area  $A$ , the flow rate is  $Av$ , and the power in this airflow with speed  $v$  is:

$$P_v = \frac{1}{2} \rho A v^3. \quad (2.5)$$

The average energy in the wind can be computed by taking the integral of Eq. 2.5 during a certain time interval  $T_p$ , which is normally one year [1].

$$\text{Averagr Energy} = \frac{1}{2} \rho A \int_0^{T_p} v^3. \quad (2.6)$$

The energy distribution at different wind speeds is identified as the power density and represented in Fig. 2.2. It is observed from Fig. 2.2 that higher amounts of wind energy are experienced when the wind speeds are above average, while the average energy occurs when the wind speed is equal to 11.2 m/s [1].

### 2.1.3 The Turbulence

Wind can hardly have constant speed in terms of magnitude and direction. The fluctuations of wind speeds with frequencies higher than the spectral gap is defined as turbulence. Turbulence has a small effect on the annual energy capture, yet it has major incidence on aerodynamic loads and power quality. Wind turbulence at a given point is defined in terms of the means of its power spectrum and can be described by one of the most commonly used models: Karman spectrum and Kaimal spectrum. The former model can be represented by [13]:

$$\phi(\omega) = \frac{K_V}{(1+(\omega T_V)^2)^{5/6}}. \quad (2.7)$$

while the latter model is given by [14]:

$$\phi(\omega) = \frac{K_V}{(1+\omega T_V)^{5/3}}. \quad (2.8)$$

The parameters  $K_V$  and  $T_V$  represent the turbulence power and the frequency bandwidth of the turbulence respectively, while  $\omega$  is associated with the wind speed frequency. Both  $K_V$  and  $T_V$  mainly depend on the mean wind speed and the surrounding terrains in the environment.

## 2.2 The Wind Turbine

Wind turbine technology is utilized to convert part of the wind kinetic energy into mechanical energy through a mechanical device called the wind turbine. This section briefly discusses the main design characteristics and aerodynamic properties of wind turbines. Fig. 2.3 represents the wind turbine diagram along with its main components such as the hub, blades, low and high speed shaft, gearbox, generator, nacelle, and tower [21].

### 2.2.1 Wind Turbine Rotor Design

The most important part of the wind turbine design is the rotor which is rotated by the propulsion of the lift and drag forces that are caused by the interaction of the rotor with the wind [1, 4, 5]. Wind turbines can be designed with different rotor axis positions such as vertical-axis and horizontal-axis rotors as shown in Fig. 2.4 [1].

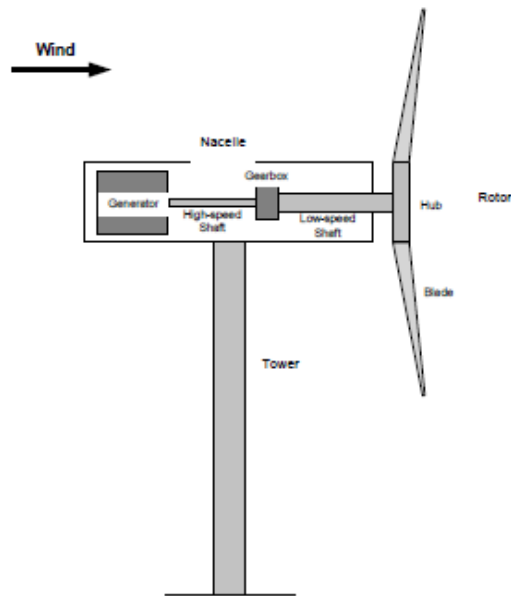


Figure 2.3: Wind turbine diagram

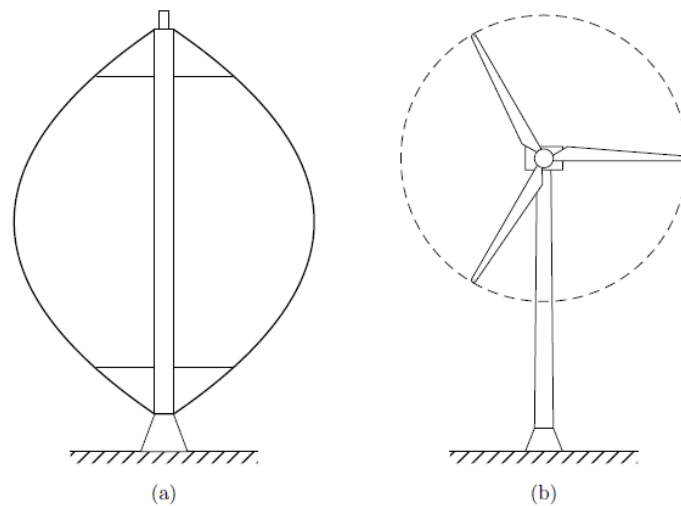


Figure 2.4: (a) Vertical-axis and (b) horizontal-axis wind turbines [1].

Fig. 2.4 (a) exhibits the Darrieus rotor which is considered the most successful vertical-axis wind turbine [1]. The generator and transmission devices are located on the ground which makes it easier to reach. Moreover, this type of turbines can capture the wind flow regardless of its direction and without the need to yaw. However, the main disadvantage of this design is the low energy capture as the rotor

intercepts with the low-height winds that have less kinetic energy as described earlier. In spite of the low-level placement of the generator and transmission devices, the maintenance process is infeasible as the rotor has to be removed [1]. Accordingly, the popularity of vertical-axis wind turbines has decreased during the last years [15, 16]. Fig 2.4 (b) represents the most commercially successful wind turbine design with a horizontal-axis three-bladed rotor [1]. The high-level wind layers have more kinetic energy and lower turbulence which results in higher energy capture by the rotor located on the top of a tower [4]. Normally, in order to capture the maximum possible energy, the rotor is yawed in the direction facing the wind. Finally, the wind turbine power electronics are placed at ground level. Wind turbines can also be classified, according to the rotor and generator rotational speed, as fixed speed as shown in Fig. 2.5, or variable speed as shown in Fig. 2.6 [21, 22]. Hence, control systems are utilized to hold or adjust the rotational speed in order to maximize the power capture.

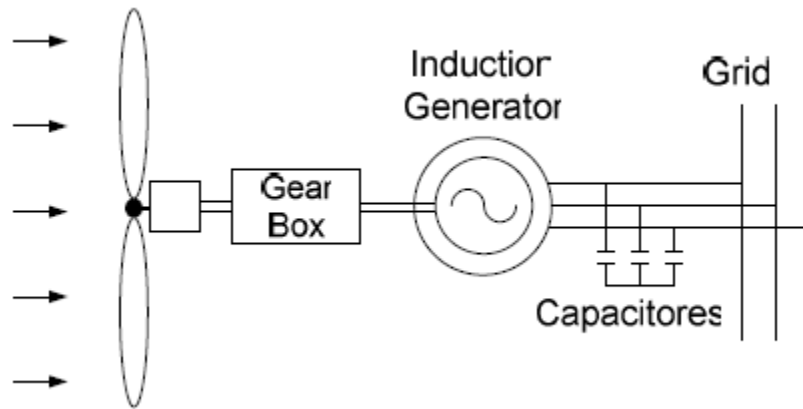


Figure 2.6: Fixed speed wind turbine generator [22]

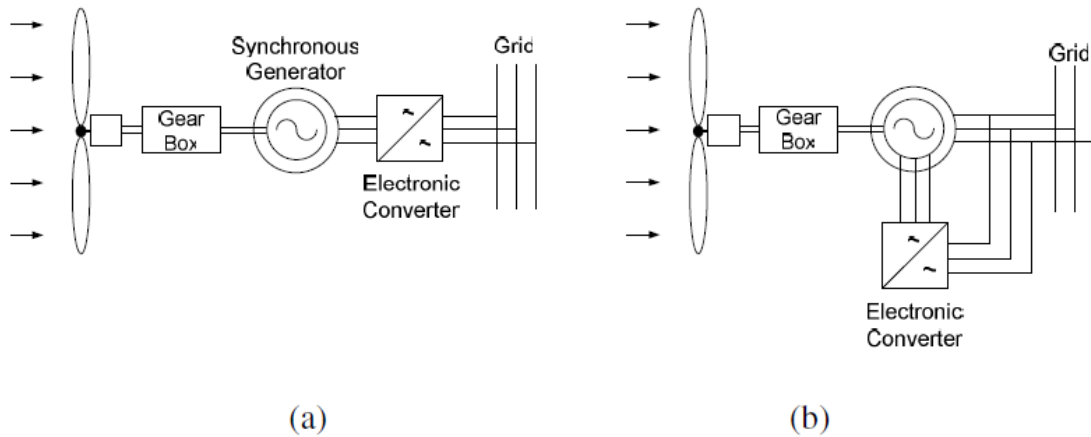


Figure 2.5: Variable speed wind turbine generators; (a) with synchronous generator, (b) with doubly fed induction generator (DFIG) [22]

## 2.2.2 Wind Turbine Aerodynamics

As mentioned earlier, wind power has become an essential power source for many countries that aim to replace the fossil and nuclear energy by clean energy resources. Wind turbines are used to generate useful mechanical energy from the wind kinetic energy, hence, it is very important to study the wind turbine aerodynamics. The term aerodynamics is used to describe the forces caused by the airflow on the wind turbines [17].

The aerodynamic models are mainly derived using two major approaches which are the actuator disc model and the blade element model [18, 19]. The actuator disc model is used to study the process of energy extraction and to provide an upper-bound limit for the maximum possible energy conversion efficiency. The blade element model provides a description of the aerodynamic conditions such as stall and explains the aerodynamic loads. It is also used to derive the torque, the captured power and the axial thrust force experienced by the turbine.

## 2.2.3 Force, Torque and Power

The thrust force on the rotor ( $F_T$ ), the total aerodynamic torque by the turbine ( $T_T$ ) and the power ( $P_T$ ) are expressed in terms of non-dimensional thrust ( $C_T$ ), torque ( $C_Q$ ) and power ( $C_P$ ) coefficients in the equations below [1]:

$$F_T = \frac{1}{2} \rho \pi R^2 C_T(\lambda, \beta) V^2, \quad (2.9)$$

$$T_T = \frac{1}{2} \rho \pi R^3 C_Q(\lambda, \beta) V^2, \quad (2.10)$$

$$P_T = C_P(\lambda, \beta) P_V = \frac{1}{2} \rho \pi R^2 C_P(\lambda, \beta) V^3, \quad (2.11)$$

where  $\rho$  is the air density,  $R$  is the rotor radius,  $\lambda$  is the tip-speed ratio,  $\beta$  is the pitch angle, and finally  $V$  is the wind speed. The torque and power coefficients are directly proportional to each other as represented in the equation below:

$$C_Q = C_P / \lambda. \quad (2.12)$$

They are also considered as essential parameters for wind turbine control systems purposes. In Wind turbines, that are designed for fixed pitch operation,  $C_Q$  and  $C_P$  become functions of  $\lambda$ , since  $\beta = 0$  naturally. Fig. 2.7 shows typical values of the coefficients  $C_Q(\lambda)$  and  $C_P(\lambda)$  of fixed-pitch turbines in two-dimensional graphs. It is observed from Fig. 2.7 that the maximum value of the power coefficient  $C_P$  occurs at  $(\lambda_o, \beta_o)$ , when the pitch angle  $\beta_o$  has a very small value, ideally zero. However, having

$\beta_o \sim 0$  leads to a very low power capture in case of any deviation in the pitch angle. Nevertheless, the maximum energy conversion efficiency can be achieved at  $\lambda_o$ . Hence, fixed-speed turbines can accomplish the maximum efficiency just at certain wind speed value, while variable-speed turbines can operate with maximum efficiency for a wide range of wind speed values. The variable-speed operation is appreciable only when the rotational speed is initially adjusted proportional to the wind speed which leads to maintaining an optimum tip-speed-ratio. Moreover, It can be concluded from Fig. 2.7 that the maximum torque coefficient can be achieved at  $(\lambda_{Q_{\max}}, \beta_o)$ , with  $\lambda_{Q_{\max}} < \lambda_o$ .

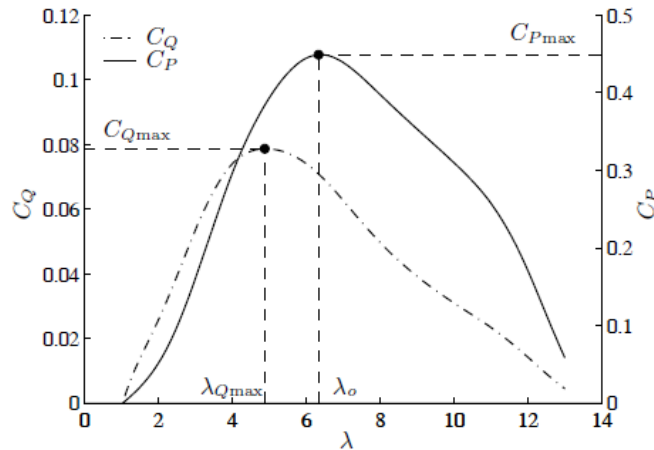


Figure 2.7: Typical variations of  $C_Q$  and  $C_P$  for a fixed-pitch wind turbine [1].

Fig. 2.8 represents both aerodynamic torque and power vs. rotor speed with the wind speed and the pitch angle as parameters, respectively. The thick line represents the locus of maximum power efficiency ( $\lambda = \lambda_o$ ). It is also noticed that maximum torque and power are achieved at different rotor speeds. For example, maximum aerodynamic torque occurs at low rotor speeds.

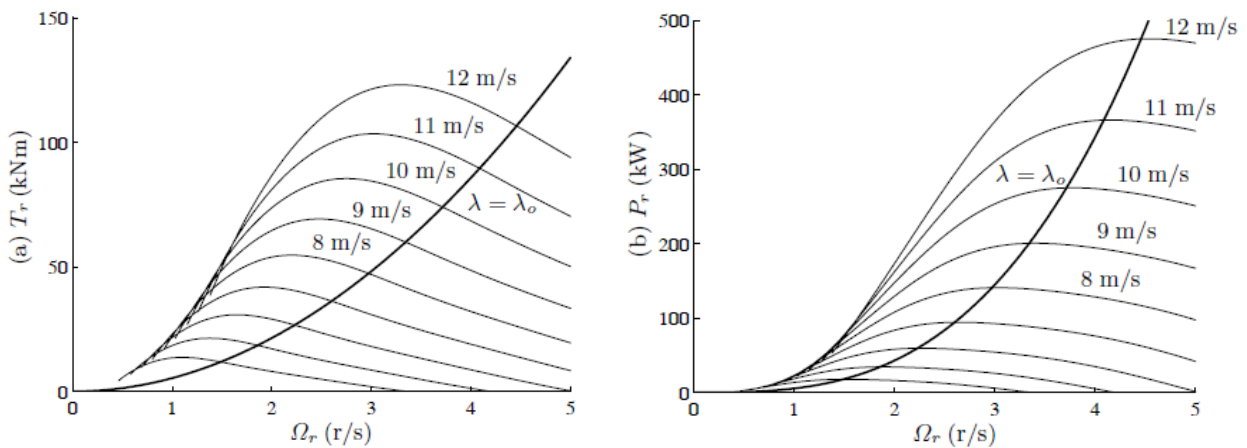


Figure 2.8: (a) Aerodynamic Torque and (b) Power VS rotor speed with wind speed as a parameter and  $\beta = 0$  [1].

## 2.3 Power Capture by Wind Turbines

As mentioned in section 2.1.2, the total power content in the wind can be evaluated using Eq. (2.13), however, only certain portion of this power can be utilized and converted into mechanical energy. Theoretically, the power extraction efficiency in wind is represented by the Power Coefficient ( $C_p$ ) which is the ratio of power captured by the turbine to the total power of the wind  $C_p = P_T/P_v$  [9]. Hence, the total power capture by the wind turbine is represented by:

$$P_T = P_v C_p = \frac{1}{2} \rho A V^3 C_p. \quad (2.13)$$

Note that the captured power should always be smaller than the wind power by having  $C_p < 1$ . Moreover,  $C_p$  can never be equal to 1, in other words, it is impossible to achieve a 100% efficiency [20]. According to Betz theory, the upper limit of the value of  $C_p$  is equal to 16/27, which means that a maximum of 59% of the wind power can be successfully extracted by a conventional wind turbine [9], [20], [22].

Another important approach used to evaluate the wind power efficiency is called the Capacity Factor (CF) [9]. The capacity factor, represented in Eq. (2.14), refers to the actual energy ( $E_{actual}$ ) generated by the wind turbine to the total energy that can be potentially generated under ideal environmental conditions ( $E_{ideal}$ ).

$$CF = \frac{E_{actual}}{E_{ideal}} \quad (2.14)$$

The capacity factor mainly depends on the design characteristics of the wind turbine and the environmental site. The most common value of the CF for a practical project is 30%, which can reach up to 50% in some conditions with good wind resource.

## 2.4 The Impact of Wind Turbines on the Grid

The continuously growing populations and the rapidly developing industries are increasing the demand for energy that is highly required to satisfy the modern standards of human needs. Therefore, renewable energy sources have been incorporated in modern power systems to contribute in power production and to compensate for the growing energy gap. Particularly speaking, the power generated by wind turbines can affect the power systems operational security, reliability and efficiency [23], [24]. Hence, studying



the consequences of the dynamic interaction between wind farms and electrical power systems is a crucial step before the real integration of wind farms into the grid. Due to the high variations in the wind power generation at different timescales: hourly, daily, or seasonally, maintaining grid stability is considered highly challenging. These power variations result in voltage variations that can cause serious problems in the voltage stability, static security, and transient stability [23]. In order to achieve a reliable service, stable frequency, and to compensate for uncertainty and variability caused by wind turbines, several operating reserves are used by power system operators [24]. The incorporation of wind turbine farm has some impacts on the power system operation point, the load flow of real and reactive power, the nodal voltages and power losses.

Adding wind power to power systems will also have some benefits on the grid such as reducing both emissions caused by electricity production and operational costs of the power system due to the consumption of lower amounts of fuel in conventional power plants [23]. On the other hand, the most serious disadvantage of wind turbines on power systems is the fluctuations and the difficulties in power predictions [25]. These fluctuations of power have a huge impact on the grid stability. To overcome such problems, grid requirements have been studied in the literature with concentration on the fault ride-through and power control capabilities of large wind farms [26].

#### **2.4.1 Location**

The location of the wind farms relative to the load, and the relationship between wind power production and load consumption have huge impacts on power systems [23- 25]. For example, wind power produced by the plant can affect the direction of the power flow in the network and might even reverse its direction at some parts of the grid. These changes in the use of power lines can cause either power losses or can add benefits. Grid extensions are usually installed in weak grids in order to maximize the use of the wind power generated by wind turbines located far from load centers. Accordingly, the cost of grid reinforcements highly depends on the relative location of wind power plants to the load and grid infrastructure [24].

#### **2.4.2 Generators**

Power systems are also influenced by the type of wind turbine generator system. The two main generators used for wind power applications are fixed speed and variable speed wind generator.

- **Fixed Speed Wind Generator**

In the early years of wind power systems development, fixed speed wind turbines and induction generators were the most commonly used in wind farms. A fixed speed wind generator normally consists of squirrel cage induction generator that is directly connected to the grid with limited speed variations. In this type of generators, the power can only be controlled through pitch angle variations [24]. Since the wind turbine efficiency mainly depends on the tip-speed ratio, the power of a fixed speed wind generator is directly proportional to the wind speed [23]. Since the generator is considered as an induction machine that does not have reactive power control capabilities, power factor correction systems are usually utilized to compensate for the reactive power demand of the generator. Fig. 2.5 represents the schematic diagram of the fixed speed induction generator.

- **Variable Speed Wind Generator**

Unlike the fixed speed generators, the variable speed concepts ensure that the wind turbine operates at the optimum tip-speed ratio and accordingly this will result in achieving the optimum power coefficient for a wide wind speed range. The most popular variable speed wind generator is the Doubly-Fed Induction Generator (DFIG). DFIG is equipped with a wound rotor induction generator that has a voltage source converter connected to the slip-rings of the rotor. As shown in Fig. 2.5 (b), the grid is directly coupled to the stator winding while the power converter is connected to the rotor winding. The DFIG can operate in two different modes depending on the wind speed. During low wind speeds, the rotor rotational speed drops and leads the generator to operate in a sub-synchronous mode in which the rotor absorbs power from the grid. On the other hand, in the case of high wind speed, the rotor runs at super synchronous speed which will eventually deliver power to the grid through the converters. It is concluded that the variable speed generators are capable of supplying higher amount of energy to the network while maintaining lower power fluctuations.

### **2.4.3 Wind turbine impact on voltage stability and power quality of the grid**

Maintaining synchronism of power systems when a serious disturbance occur, such as a switching circuits elements ON and OFF, highly depends on the grid transient stability.

System stability is directly related to power system faults in a network such as grid transmission lines tripping, production capacity losses and short circuits. Such failures affects the active and reactive power balance and reverse the direction of power flow. Large voltage drops might take place in power systems even though the operating generators capacity is high enough to satisfy the demand. Any

unbalance of active and reactive power in the system might lead to a voltage variations that exceed the stability limits [23]. This voltage instability might take place and cause tripping in the circuit and may extend to be a complete blackout. In the early stage of the wind power development, only a small number of wind turbines were connected to the power network. In this case, if any voltage drop occurred due to a fault somewhere in the grid, the wind turbine was eliminated from the power system and was connected again when the fault was over by compensating for the voltage drop [24]. Supplying discontinuous amount of power to the grids can have potential impact on power quality. For example, when low wind power penetrations occur in the grid system, wind farms become active power generators that are accompanied by control systems at the conventional plants. On the other hand, at high penetrations when wind speeds are either below cut-in or above furl-out, the grid disconnects the wind turbines to keep them in idle mode [24]. When the wind speed gets back to its accepted operation range, the turbines get reconnected. It is important to mention that the immediate reconnection of a large power generator might cause a brownout to the system due to the required current that magnetizes the generator [24]. This current usually results in a power peak when the generator starts feeding active power to the grid. In certain scenarios, wind power output exceeds the load in the consumer side, which leads to increasing the voltage above the grid threshold. Voltage fluctuations occur in the grid in response to the short-term wind power variations. These rapid voltage fluctuations are called “flicker” due to its impact on light bulbs. Flicker can cause serious damage to the electrical and electronics equipment of the power system. In a weak grid where the voltage has rapid variations, flicker can be produced even if only a single turbine is connected to the network. Moreover, consumers’ electrical devices have the ability to produce harmonics that can get magnified by wind turbine operations [24]. Transient instabilities can be introduced to the grid in response to the action of wind farms in case of an electrical fault. Control systems might not have the ability to overcome such instabilities in the network. These problems are mainly noticed when a huge wind power is supplied to a low voltage grid. On the other hand, in stronger grids, voltage variations are barely noticed due to the low impedance of the network. Frequency variations might occur as a results of several conditions such as: wind speed variations, connections and disconnections of wind turbines, and the imbalance between the amount of generated power and the demand on the load side [23].

Table 2.2: Summary of different problems related to the power quality [23]

| Characteristics                      | Description   | Cause   |
|--------------------------------------|---|---|
| <b>Voltage Variations</b>            | Change of the voltage effective value during several minutes or more                                  | Average production of wind power  |
| <b>Flicker</b>                       | Voltage fluctuations in frequencies between 0.5 Hz and 30 Hz  | <ul style="list-style-type: none"> <li>• Change operations</li> <li>• Shadow tower effect</li> <li>• Failure of the rotor orientation</li> <li>• Shear effect</li> <li>• Wind speed variations</li> </ul> |
| <b>Harmonics and inter-harmonics</b> | Voltage fluctuations in frequencies between 50 Hz (60 Hz for the north America countries) and 2.5 kHz | <ul style="list-style-type: none"> <li>• Frequency converters</li> <li>• Thyristor controllers</li> <li>• capacitors</li> </ul>   |
| <b>Power factor</b>                  | Reactive power consumption  | Inductive components  |

## 2.6 Literature Review

Doubly fed induction generators (DFIG) are extensively used in wind energy conversion systems such as wind turbines. The DFIGs dynamic characteristics requires creating high-performance control schemes. Nevertheless, the dynamic features of such generators mainly depend on certain nonlinear parameters, such as stator flux, stator current, and rotor current, which makes the overall system more complex. Hence, robust controllers are required to be designed in such systems in order to support the dynamic frequencies of wind energy to maintain system stability and good performance. In general, conventional control designs such as the proportional-integral (PI) controllers have multiple disadvantages, such as difficulties in tuning parameters, average dynamic performance, and reduced robustness [33].

Different DFIG wind turbine control strategies have been widely studied in the literature; such as pitch angle control methods, rotor voltage/current control, torque control, internal and de-loaded control for frequency regulations, and reactive and active power control.

In [34], a new rotor current scheme that is implemented in the positive synchronous reference frame is developed. The control system is designed of a standard PI controller and a generalized AC integrator. Their results show that the proposed control scheme leads to significant elimination of either DFIG power or torque oscillations under distorted grid voltage conditions.

In [35], a model predictive rotor current control (MPRCC) method is proposed to track the rotor reference current through deriving the reference rotor voltage. The results presented a sinusoidal and balanced rotor currents under both balanced and unbalance network.

However, none of the aforementioned references discussed the initial rotor current overshoot/undershoot and the steady state error of the system response. Moreover, it is clear that only conventional control methods are implemented in their designs.

Hamane et al [36], presented a comparative analysis of PI, Sliding Mode and Fuzzy-PI controllers for DFIG wind energy conversion system. The results show that, with Fuzzy PI, the settling time is massively reduced, peak overshoot of values are limited and oscillations are damped out faster. Nevertheless, their proposed decoupled regulation method focuses on controlling the active and reactive power rather than the rotor current of the DFIG.

Several works in the literature have discussed and proposed neural network based controllers for a DFIG-based wind turbines [43]-[47]. Tang et al. [48], presented a neural network based controller for the reactive power control of wind farm with DFIG to damp the oscillation of the wind farm system after the ground fault of the grid. Medjber et al. [49], proposed a strategy that uses neural networks and fuzzy logic controllers to control the power transfer between the machine and the grid using the indirect vector control and reactive power control techniques. Soares et al. [50], presented neural networks based controllers to control the active and reactive power of the DFIG, and then compared the results between proportional-integral controllers and neural networks based controllers. The results show that better dynamic characteristics can be obtained using neural networks based controllers. However, there is no work in the literature that presents neural network control of DFIG rotor current.

Moreover, [37] proposed a classical PI and Fuzzy-PI controller design to perform decoupling control of active and reactive powers for DFIG. The results shows that the Fuzzy-PI controller reduces the settling time considerably, limits peak overshoot and damps oscillations faster compared to the conventional PI Controller.

Belgacem et al. [51], presented DFIG current control schemes in order to regulate the active and reactive powers exchanged between the machine and the grid. The authors compared between conventional PI and FLC controllers in terms of reference tracking and speed disturbance rejection.

However, the paper did not compare the differences between PI controller and FLC in terms of overshoot/undershoot, settling time and steady state error of the rotor current neither extracted power using the proposed controllers. Moreover fuzzy-PI controller was not introduced in this work.

In [38], a Fuzzy-PI controller scheme is proposed to control the active and reactive power of wind energy conversion systems with DFIGs. It is concluded from the results that using the proposed Fuzzy PI controller improves the dynamic response of the system by achieving faster response with almost no overshoot, shorter settling time and no steady-state error.

Hence, most of the work reported in the literature investigates either the effects of the conventional controller on the rotor current of the DFIG, or the effects of PI Fuzzy controller on other DFIG features such as active and reactive power. However, to our knowledge, utilizing the fuzzy logic controller in order to minimize the overshoot/undershoot, settling time and steady state error of the rotor current has not been studied.

## Chapter 3 : Modeling Wind Turbines

The studied model consists of a single two-mass wind turbine that is connected directly to the power system. It is assumed that the wind turbine has a general model consisting of electrical, aerodynamic, mechanical, electrical, and control systems. Fig. 3.1 represents the structure of the wind turbine model [39]. A wind speed model is also studied to estimate the equivalent wind speed that is fed to the aerodynamic model. The mechanical system model provides the wind model with information regarding the turbine rotor position in order to consider the tower shadow, the rotational turbulence, and the wind speed variations over the rotor disk. In addition to the equivalent wind speed, the aerodynamic model is also fed with the pitch angle from the control system and the speed of the turbine rotor from the mechanical model. On the other hand, the aerodynamic model is responsible of computing the aerodynamic torque that fed into the mechanical model along with the generator speed from the electrical model [39]. The mechanical model output is the mechanical turbine power that is considered as an input to the electrical model. The electrical model is responsible of delivering the output currents to the power system through the wind turbine terminals while receiving input voltages from the power system. The input signals to the control system are: 1) the hub wind speed from the wind model, 2) the generator speed from the electrical model and, 3) the active and reactive powers,

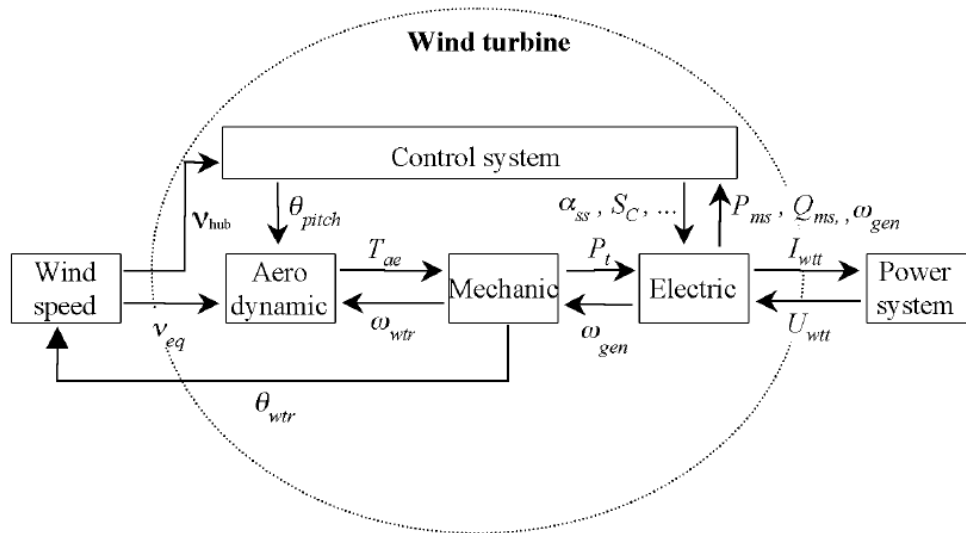


Figure 3.1: General structure of the wind turbine model. [39]

which represent the measured voltages and currents of the control system from the electrical model. The control system output signals are: 1) the pitch angle to the aerodynamic model, 2) the soft-starter angle to the electrical model and, 3) the capacitor bank switch signals to the electrical model [39].

### 3.1 Wind Speed Model

Wind speed varies from time to time and from one location to another. This variation highly affects the angular speed and torque of the wind turbine rotor and hence it has direct relation to the amount of the power capture by the wind turbine [40]. Therefore, in order to properly simulate the WTGS dynamics, it is important to study the wind speed model. The approach of wind speed modeling in this work depends on summing up all four components of the wind speed namely: 1) constant component representing the average wind speed  $v_{wa}(t)$  2) ramp component  $v_{wr}(t)$  3) gust component  $v_{wg}(t)$  and 4) turbulence component  $v_{wt}(t)$  as shown in the equation below [34, 35]:

$$v_w(t) = v_{wa}(t) + v_{wr}(t) + v_{wg}(t) + v_{wt}(t). \quad (3.1)$$

The wind speed ramp component can be calculated using the following equation:

$$v_{wr}(t) = \begin{cases} 0, & t \leq T_{r1} \\ A_r \left( \frac{t - T_{r1}}{T_{r2} - T_{r1}} \right), & T_{r1} < t \leq T_{r2}, \\ A_r, & t > T_{r2} \end{cases} \quad (3.2)$$

Where  $T_{r1}$  and  $T_{r2}$  are the times representing the starts and ends of the ramp respectively, and  $A_r$  is the ramp maximum amplitude. The gust component simulates any abnormal temporary increase of the wind speed and it is represented by:

$$v_{wg}(t) = \begin{cases} 0, & t < T_{g1} \\ A_g \left( 1 - \cos \left[ 2\pi \left( \frac{t - T_{g1}}{T_{g2} - T_{g1}} \right) \right] \right), & T_{g1} \leq t \leq T_{g2} \\ 0, & t > T_{g2} \end{cases} \quad (3.3)$$

Where  $T_{g1}$  and  $T_{g2}$  are the times representing the starts and ends of the gust respectively, and  $A_g$  is the ramp maximum amplitude. Finally, the turbulence component is represented by a signal that has a power spectral density of the form [41]:



$$P_{Dt}(f) = \frac{lv_{wa} \left[ \ln\left(\frac{h}{z_o}\right) \right]^{-2}}{\left[ 1 + 1.5 \frac{fl}{v_{wa}} \right]^{5/3}} \quad (3.4)$$

$$P_{Dt}(f) = \frac{lv_{wa} \left[ \ln\left(\frac{h}{z_o}\right) \right]^{-2}}{\left[ 1 + 1.5 \frac{fl}{v_{wa}} \right]^{5/3}} \quad (3.5)$$

where  $h$  is the wind wheel height,  $l$  is the turbulence scale which is greater than  $h$  by a factor of 20 and has a maximum value of 300 meters, and  $z_o$  is a roughness length parameter which depends on the type of the landscape as represented in Table 3.1 [41].

Table 3.1: Values of  $Z_o$  for different types of landscapes. [41]

| Landscape type                  | Range of $z_o$ (m) |
|---------------------------------|--------------------|
| Open sea or sand                | 0.0001-0.001       |
| Snow surface                    | 0.001-0.005        |
| Mown grass or steppe            | 0.001-0.01         |
| Long grass or rocky ground      | 0.04-0.1           |
| Forests, cities and hilly areas | 1-5                |

In order to generate the turbulence signal, a shaping filter is designed and applied to a flat spectrum noise signal (Additive white Gaussian noise (AWGN)). Given that the power spectral density  $P_{Dt}$  is very similar to the response of a first order filter. The transfer function of the designed filter is defined as:

$$H(s) = \frac{kK}{s+p} \quad (3.6)$$

with

$$p = \frac{2\pi((K_1^2)^{3/5} - 1)}{K_2 \sqrt{K_1^2 - 1}}, \quad (3.7)$$

$$K = K_1 p, \quad (3.8)$$

where  $K_1$  and  $K_2$  are given by:

$$K_1 = lv_{wa} \left[ \ln\left(\frac{h}{z_o}\right) \right]^{-2}, \quad (3.9)$$

$$K_2 = 1.5 \frac{1}{v_{wa}}, \quad (3.10)$$

hence the generated signal has a power spectral density of the form:

$$P_{filter} = \frac{\frac{K^2}{p^2}}{1 + \frac{4\pi^2}{p^2 f^2}}. \quad (3.11)$$

### 3.2 Aerodynamic Model

The most common technique to create aerodynamic model of wind turbine is the blade element method [41]. This technique requires long computational time, therefore it is considered unsuitable for modeling a wind farm with multiple wind turbines. In this work, an aerodynamic model that is based on the aerodynamic power coefficient ( $C_p$ ) is presented. The power coefficient, for a given rotor, depends on the pitch angle ( $\beta$ ) and on the tip speed ratio ( $\lambda$ ). The aerodynamic torque ( $T_{ae}$ ) is calculated based on the rotor radius ( $R$ ), the wind speed ( $v_w$ ), the air density ( $\rho$ ), and the power coefficient using the following equation [43]:

$$T_{ae} = \frac{\pi}{2\lambda} \rho R^3 v_w^2 C_p(\theta_{pitch}, \lambda), \quad (3.12)$$

where  $C_p$  is given by:

$$C_p = \lambda C_t, \quad (3.13)$$

where  $C_t$  is the torque coefficient, and the tip speed ratio  $\lambda$  is given by:

$$\lambda = \frac{R\Omega_t}{v_w} \quad (3.14)$$

where  $\Omega_t$  represents DFIG rotor angular speed. In this work, a 2 MW wind turbine of type Mitsubishi MWT 92, shown in Fig. 3.2, is modeled. The presented aerodynamic model is based on data taken from the manufacturer's brochures and it states as follows [43]:

- The turbine blade length is 42 meters.
- When the wind speed ranges between 11 and 13 m/s, the nominal power can be extracted.

- The angular speed of the turbine rotor (low speed shaft) ranges between 8.5 and 20 rpm.
- For the case of two- pole generator and 50 Hz grid, the selected ratio of the gearbox 100.
- The power coefficient and the tip blade maximum speed ratio are represented by the following equations, respectively:

$$C_p = 0.773 \left( \frac{151}{\lambda_i} - 0.58\beta - 0.002\beta^{2.14} - 13.2 \right) (e^{-18.4/\lambda_i}), \quad (3.15)$$

$$\lambda_i = \frac{1}{\lambda + 0.02\beta} - \frac{0.003}{\beta^3 + 1}. \quad (3.16)$$

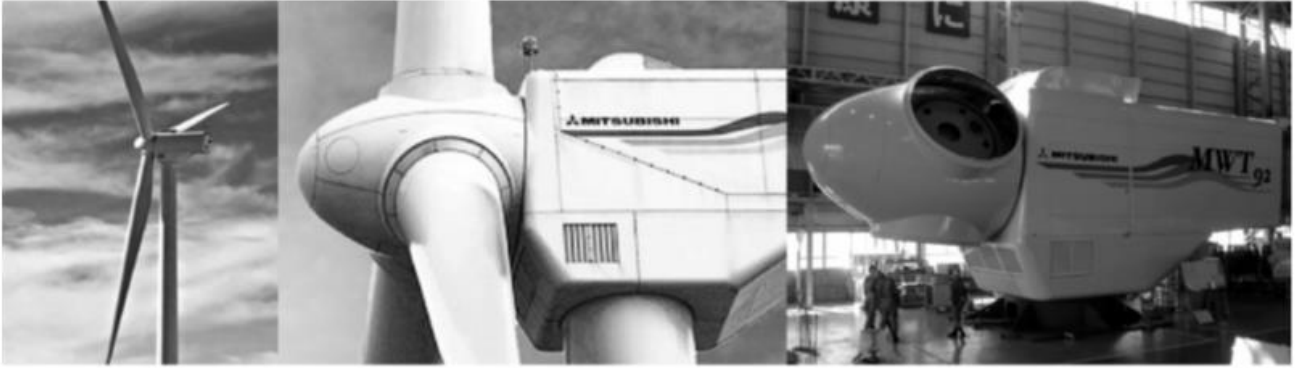


Figure 3.2: Mitsubishi MWT 92 wind turbine [43].

### 3.3 Mechanical Model

The mechanical or the drive train model in this work consists of certain parts of the dynamic structure of the wind turbine that have direct contribution on the interaction with the power system [41]. Hence, the drive train is the only considered part as it has the largest influence on the power fluctuations. The other parts such as the tower and the flap bending modes of the wind turbine are neglected. The drive train model consists of the wind wheel, the turbine shaft (low speed shaft), the gearbox, and the generator's rotor shaft (high speed shaft) [36, 37]. The aerodynamic torque on the turbine rotor is converted by the drive train into the torque on the low speed shaft. The gearbox scales down the torque from the low speed shaft to the high speed shaft. The gearbox ratio between the low speed and high speed shafts usually ranges between 50 and 150, and the inertia of the turbine rotor is usually 90% of the whole system inertia [41]. The drive train model is usually treated as a series of masses that are linked to each other through an elastic coupling that has linear stiffness, a damping ratio and a multiplication ratio. In this work, a two mass model is assumed where the wind wheel and the turbine

rotor are considered as one inertia  $J_t$  and the gearbox and the generator's rotor as another inertia  $J_m$  that are connected, with a  $k$  angular stiffness coefficient and a  $c$  angular damping coefficient, through the elastic turbine shaft. In this work, a two mass model presented in Fig. 3.3 is used. A gearbox exchange ratio  $N = 100$  is assumed and the inertia of the low speed shaft  $J_t$  and the damping coefficient  $c$  are assumed to be  $63.5 \text{ kg.m}^2$  and  $0.001$  respectively. The system dynamics are represented as:

$$\begin{pmatrix} \dot{\omega}_m \\ \dot{\omega}_t \\ \omega_m \\ \omega_t \end{pmatrix} = \begin{pmatrix} \frac{-v^2c}{J_m} & \frac{vc}{J_m} & \frac{-v^2k}{J_m} & \frac{vk}{J_m} \\ \frac{vc}{J_t} & \frac{-c}{J_t} & \frac{vk}{J_t} & \frac{-k}{J_t} \\ 1 & 0 & 0 & 0 \\ 0 & 1 & 0 & 0 \end{pmatrix} \begin{pmatrix} \omega_m \\ \omega_t \\ \theta_m \\ \theta_t \end{pmatrix} + \begin{pmatrix} \frac{1}{J_m} & 0 \\ 0 & \frac{1}{J_m} \\ 0 & 0 \\ 0 & 0 \end{pmatrix} \begin{pmatrix} \tau_{em} \\ \tau_{ae} \end{pmatrix}. \quad (3.17)$$

where  $\theta_t$  and  $\theta_m$  represent the angles of the wind wheel and the generator shaft,  $\omega_t$  and  $\omega_m$  are the angular speed of the wind wheel and the generator,  $\tau_{ae}$  is the torque applied to the turbine axis by the wind wheel and  $\tau_{em}$  is the generator torque.

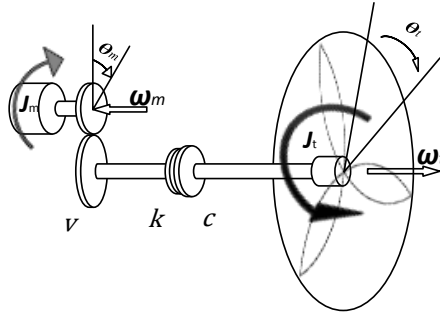


Figure 3.3: Two mass drive train model [41].

### 3.4 Electrical Model

In this work, a doubly fed induction generator with a back-to-back three phase converter are used as shown in Fig. 3.4. The main components of the DFIG are the stator and the rotor [41]. The stator is connected directly to the grid where it is supplied by three-phase voltages with constant amplitude and frequency to create the stator magnetic field [42]. On the other hand, the rotor is connected to the back-to-back converter that is connected to the grid. The grid supplies the rotor with three-phase voltages that achieve different amplitude and frequency at steady state in order to satisfy the different operating conditions of the generator [41]. Both the converter and the control system are responsible of providing the required AC voltages for the generator rotor in order to control the overall DFIG operating point.

The three phase currents and voltages are converted from the abc reference frame to the rotating dq reference frame in order to simplify its representation and control system modeling. Thus, the relations between the voltages on the generator windings and the currents and its first derivative can be studied on a synchronous reference dq frame as follows:

$$\begin{pmatrix} v_{sq} \\ v_{sd} \\ v_{rq} \\ v_{rd} \end{pmatrix} = \begin{pmatrix} L_s & 0 & M & 0 \\ 0 & L_s & 0 & M \\ M & 0 & L_r & 0 \\ 0 & M & 0 & L_r \end{pmatrix} \frac{d}{dt} \begin{pmatrix} i_{sq} \\ i_{sd} \\ i_{rq} \\ i_{rd} \end{pmatrix} + \begin{pmatrix} r_s & L_s \omega_s & 0 & M \omega_s \\ -L_s \omega_s & r_s & -M \omega_s & 0 \\ 0 & sM \omega_s & r_r & sL_r \omega_s \\ -sM_s \omega_s & 0 & -sL_s \omega_s & r_r \end{pmatrix} \begin{pmatrix} i_{sq} \\ i_{sd} \\ i_{rq} \\ i_{rd} \end{pmatrix}, \quad (3.18)$$

where  $L_s$  and  $L_r$  are the stator and rotor windings self-inductance coefficient respectively,  $M$  represents the coupling coefficient between stator and rotor windings,  $s$  is the slip and  $\omega_s$  is the nominal grid frequency. Moreover, the electromagnetic torque applied on the high speed shaft and the reactive power generated by the stator inductance are represented by Eq. 3.19 and Eq. 3.20.

$$T_{em} = \frac{3}{2} PM (i_{sq} i_{rd} - i_{sd} i_{rq}), \quad (3.19)$$

$$Q_s = \frac{3}{2} (v_{sq} i_{sd} - v_{sd} i_{sq}), \quad (3.20)$$

where  $P$  is the number of the generator poles which is equal to 2 in this work. On the other hand, the Insulated Gate Bipolar transistor (IGBT) voltage source back-to-back converter is connected between the rotor and the grid. It is composed of a rotor side converter fed by a DC bus, and a grid side converter acting as an active rectifier and connected in series to a three-phase grid as shown in Fig. 3.5 [42]. In this work, the grid side converter is assumed to be acting as a DC source for simplicity.

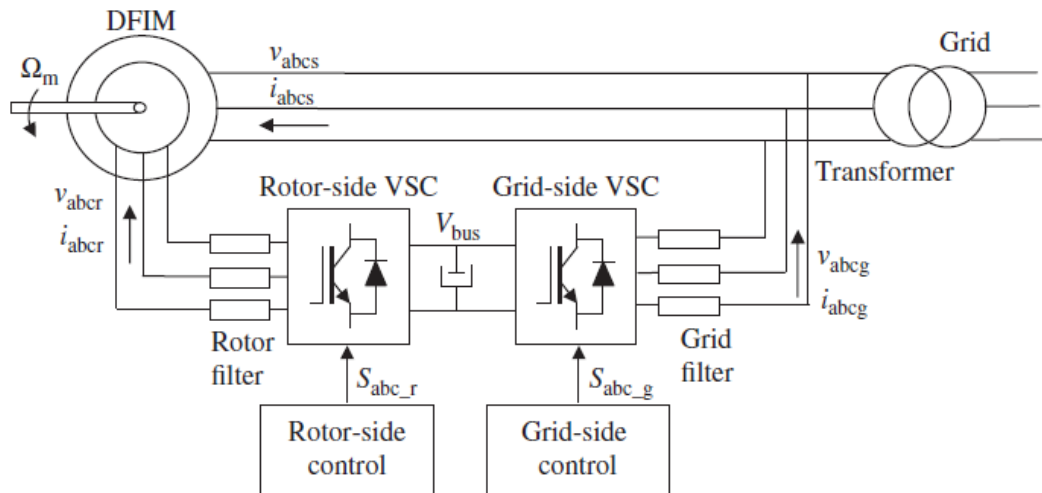


Figure 3.4: DFIM with back to back converter [42].

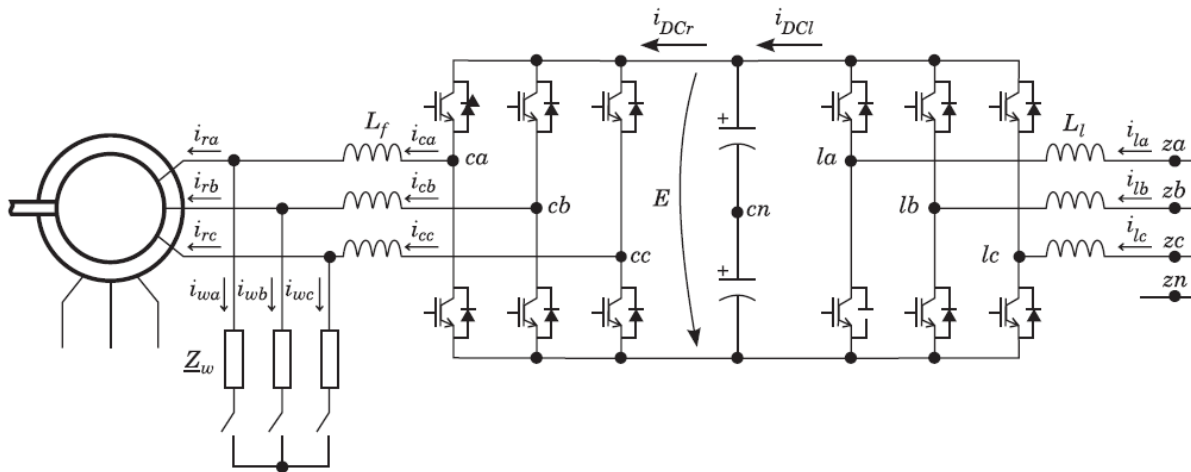


Figure 3.5: Control supply configuration for DFIM [42].

# Chapter 4 : Control System Design

## 4.1 Introduction

Control systems technology has been playing an important role in wind turbine operation. For the case of DFIG, control system is used in order to maintain magnitudes of the high-speed shaft torque, active and reactive power of the generator, and grid side converter magnitude such as the DC bus voltage and the reactive power, close to their optimum values, in order to achieve an effective energy generation. In this work, an indirect speed control is designed to force the aerodynamic torque  $T_{ae}$  to follow the maximum power curve in response to wind variations. Moreover, a rotor speed controller is designed along with a vector controller for current loops to control the rotor side converter.

### 4.1.1 Indirect speed control

One of the main objectives of the wind turbine design is generating maximum possible power supply to the grid; hence, the electromagnetic torque  $T_{em}$  should be controlled in order to force the aerodynamic torque  $T_{ae}$  to follow the maximum power curve in response to wind variations [43]. The designed controller provides the desired electromagnetic torque that corresponds to the maximum power curve. Fig. 4.1 shows the maximum power efficiency curve in which for the given constant wind speed, the operating point (a) represents the maximum efficiency [43].

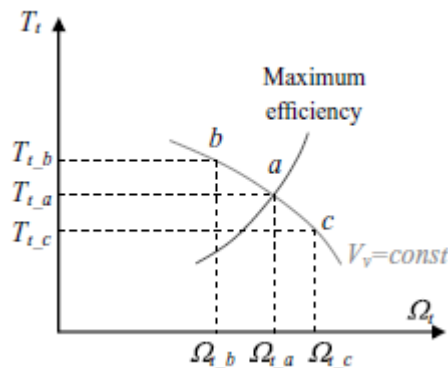


Figure 4.1: Maximum power efficiency curve [43].

The aerodynamic torque that follows the maximum power curve is given by:

$$T_{ae} = 0.5\rho\pi \frac{R^5}{\lambda_{opt}^3} C_{p\ max} \omega_m^2 = k_{opt\_t} \omega_m^2, \quad (4.1)$$

In which

$$k_{opt\_t} = 0.5\rho\pi \frac{R^5}{\lambda_{opt}^3} C_{p\ max}. \quad (4.2)$$

where  $\omega_m$  is the turbine rotor speed. In this design, certain values are given to the following variables:

$C_{p\ max} = 0.44$ , and  $\lambda_{opt} = 7.2$ . Accordingly, the controller output  $T_{em}$  can be represented by:

$$T_{em} = \frac{-k_{opt\_t} \omega_m^2}{N^3}, \quad (4.3)$$

where N is the gearbox ratio (N=100 in this work).

#### 4.1.2 Rotor side converter control

The three phase currents of the rotor and stator are initially represented by the abc reference frame which is stationary that represents three AC variables. However, the DFIG modeling requires a rotating reference frame that can be achieved by multiplying the voltage expressions by  $e^{-j\theta_s}$  and  $e^{-j\theta_r}$ , respectively to obtain the dq frame voltage expressions. Fig. 4.2 illustrates different reference frames that represent frame vector of the DFIG. The dq frame is a synchronous frame rotating at  $\omega_{sy}$  representing two dc variables. In this case, these d-axis is aligned with the stator flux space vector. Accordingly, the rotor voltages can be represented in the dq frame as a function of the rotor currents and stator flux as shown in the following equations (note that the stator flux in the q axis  $\psi_{qs} = 0$ ) [43]:

$$v_{dr} = R_r i_{dr} + \sigma L_r \frac{d}{dt} i_{dr} - \omega_r \sigma L_r i_{qr} + \frac{L_m}{L_s} \frac{d}{dt} |\vec{\psi}_s| \quad (4.4)$$

$$v_{qr} = R_r i_{qr} + \sigma L_r \frac{d}{dt} i_{qr} - \omega_r \sigma L_r i_{dr} + \omega_r \frac{L_m}{L_s} |\vec{\psi}_s|, \quad (4.5)$$

where  $R_r$ ,  $L_r$  and  $\omega_r$  are the rotor resistance, inductance and frequency, respectively,  $L_s$  and  $\vec{\psi}_s$  are the stator inductance and flux, respectively. The  $\sigma$  is given by:

$$\sigma = 1 - \frac{L_m^2}{L_s} L_r, \quad (4.6)$$



where  $L_s$  and  $L_m$  represent the stator inductance and the mutual inductance, respectively [43]. In simulation, the dq rotor current control can be performed by simply adding controllers for each current component as represented in Fig. 4.2. Moreover, in order to assist these controllers, the cross terms of the previous two equations can be used at the output of each controller. To achieve synchronization between the grid and the stator, a simple phase-locked loop (PLL) can be used [42]. The PLL helps in providing robustness to the estimation and a rejection of small disturbances or harmonics. In this work, the reference generation strategy is based on zero current reference of the rotor in the d direction ( $i_{dr} = 0$ ). Hence, by setting the  $i_{dr}$  reference ( $i_{dr}^*$ ) equal to zero and by integrating a PI controller into the system, the  $i_{dr}$  component should go to zero at the steady state. Moreover, another PI controller is integrated into the system in order to control the  $i_{qr}$  component to reach its optimum reference value given by:

$$i_{qr}^* = \frac{-2}{3} T_{em} p \frac{L_m}{L_s} |\vec{\psi}_s| \quad (4.7)$$

The block diagram shown in Fig. 4.2 represents the control system using PI controllers for both  $i_{dr}$  and  $i_{qr}$ .

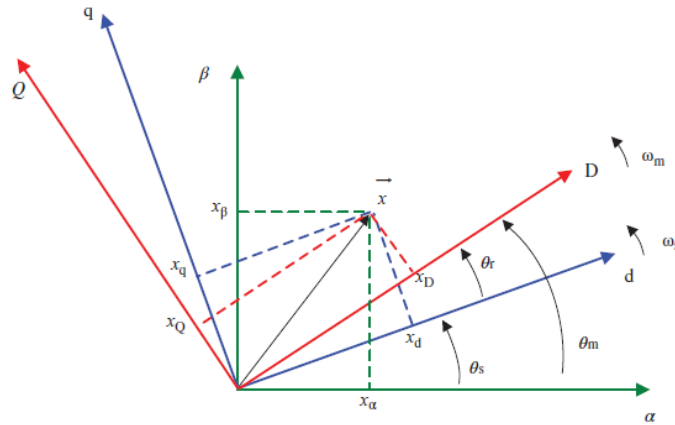


Figure 4.2: Different reference frames that represent space vectors of DFIG [42].

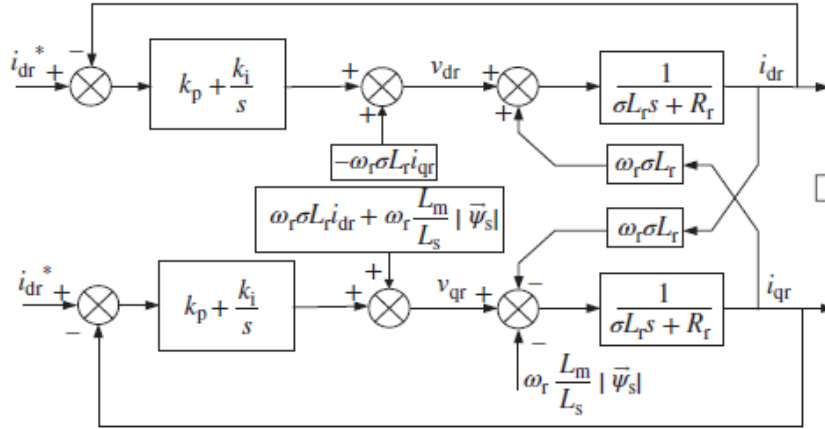


Figure 4.3: Second-order system of closed-loop current control with PI controllers [42].

The second order transfer function of the closed-loop system  $i_{dr}$  and the  $i_{qr}$  shown in Fig. 4.3 is represented below:

$$\frac{i_{dr}}{i_{dr}^*} = \left( \frac{sk_p + k_i}{\sigma L_r s^2 + (k_p + R_r)s + k_i} \right) \quad (4.8)$$

$$\frac{i_{qr}}{i_{qr}^*} = \left( \frac{sk_p + k_i}{\sigma L_r s^2 + (k_p + R_r)s + k_i} \right) \quad (4.9)$$

## 4.2 Proportional-Integral Control

In this analysis, a variable speed wind turbine rated at 2 MW is studied. Mitsubishi started with the VSWT DFIG based technology with model MWT92 rated at 2MW. Then it offered models MWT 95, 100, and 102 rated at 2400kW and MWT92 rated at 2300kW. Fig. 4.4 (a) represents the power coefficient ( $C_p$ ) VS the tip speed ratio ( $\lambda$ ) while (b) exhibits the generated power VS the wind speed for the 2 MW Mitsubishi design.

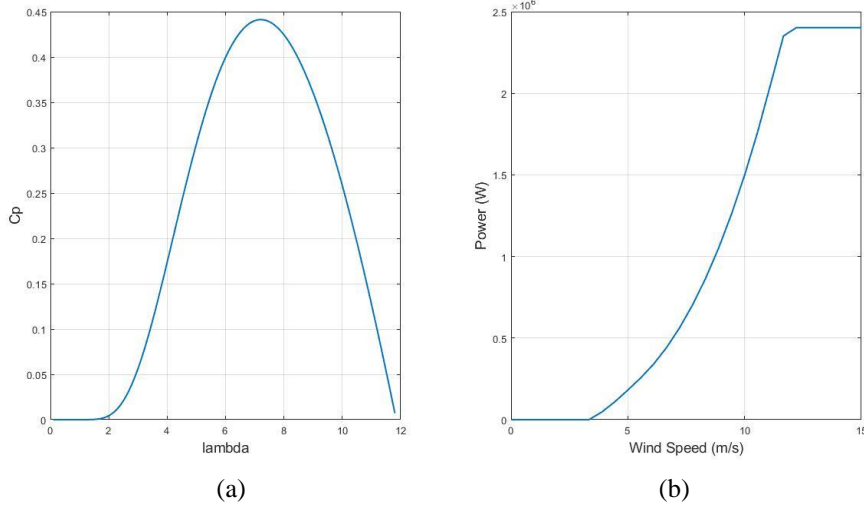


Figure 4.4: (a) the power coefficient ( $C_p$ ) VS the tip speed ratio, (b) the generated power Vs. the wind speed for the 2 MW Mitsubishi design [43].

The designed system is verified by comparing the extracted power values of three different wind speeds with the extracted power represented in Fig. 4.4 (b). Table 4.1 shows the three wind speeds and their corresponding power values.

Table 4.1: Wind speed values with their corresponding generated power values.

| Wind Speed (m/s) | Power (MW) |
|------------------|------------|
| 7.2              | 0.5642     |
| 10               | 1.498      |
| 13.3             | 2.402      |

The PI controller was designed using a built-in PID controller block in Simulink. The values of the PI controller coefficients,  $k_p$  and  $k_i$  for both rotor current components, were tuned until the desired control gains were obtained. Note that  $k_p$  has the same value for both controllers as well as  $k_i$ .

$$k_p = 0.5771$$

$$k_i = 491.5995$$

Moreover, the electromagnetic torque PI controller that works as an indirect speed controller is designed by choosing the following coefficients of the regulator:

$$k_p = 5080$$

$$k_i = 203200$$

### 4.3 Fuzzy Control

Fuzzy logic controller was first introduced by Zadeh in 1965. After that, Mamdani presented new concepts of controllers that are based on fuzzy logic in 1974 [27]. The main concept behind the fuzzy logic is studying analog inputs in terms of logical variables that can take continuous values between 0 and 1. Fuzzy logic control is considered, in many occasions, more effective than the conventional control, especially in large-scale systems. It is usually adopted in electronics systems in order to enhance the system performance by minimizing the fluctuations of the system outputs [28, 29]. Fuzzy logic is mainly based on the element ( $x$ ) and the associated membership function ( $\mu$ ) which determines the percentage of this element belonging to the fuzzy set [30]. A general fuzzy set ( $A$ ) is represented by a membership function  $\mu_A$  and the element which can have any value in the range ( $X$ ) as represented in the equation below.

$$A = \{(x, \mu_A(x)) | x \in X\}. \quad (4.10)$$

Multiple variables can belong to the same subset ( $A$ ) or to different subsets ( $A$  and  $B$ ) but with different percentages. The members of these subsets represent the values of each variable. The membership functions are created with certain shapes that are defined in a specific range. Fig. 4.5 represents an example of a triangular membership function that has a range of  $(-E, E)$ .

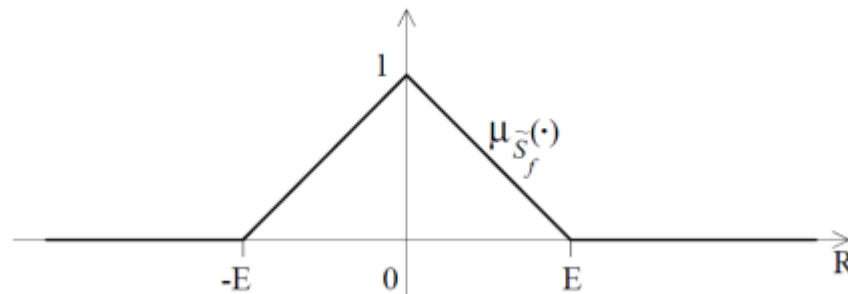


Figure 4.5: A triangular membership function

At  $x = 0$ , the membership function has a value of 1 which illustrate that this value belong to this membership function with a percentage of 100%. On the other hand, at  $x = \frac{E}{2}$ , the membership has a value of 0.5 which means that there is a chance of 50% in which this variable can belong to this membership function [31]. When designing a fuzzy logic control, we should pass by three phases: 1) Fuzzification, 2) Fuzzy rule base, and 3) Defuzzification. The former phase includes designing the membership functions and selecting the proper range. The middle phase represents the rules that link

the inputs to the outputs, and they are square of the number of the designed memberships. The latter phase transforms the generated fuzzy value into a numerical value. A general fuzzy logic block diagram is represented in the Fig. 4.6.

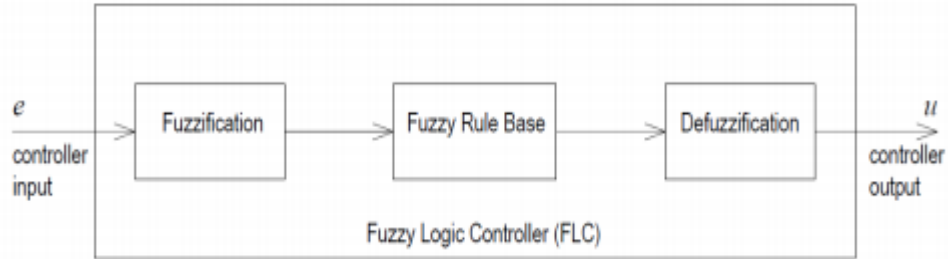


Figure 4.6: The three phases of the fuzzy logic controller.

Fuzzy logic controllers can be easily implemented in different systems, as they do not require a knowledge of the system mathematical model [32]. In this thesis, the fuzzy logic controller is implemented because it has the ability to cope with the nonlinearities and the uncertainties of the system that the PI cannot deal with alone. However, the fuzzy logic controller along with the PI helped in enhancing the designed system by almost eliminating the overshoot and minimizing the settling time and the steady state error. In this work, two inputs are chosen for the fuzzy logic controller; the system frequency error and the one-step delayed error. The membership functions are designed to satisfy the best response results. The range of both inputs is chosen to be  $[-80000 \ 80000]$  and the output range is set to  $[-90 \ 90]$  as exhibited in Fig.4.7 and 4.8, respectively. The design consists of seven triangular membership functions for both inputs and nine triangular functions for the output. The FLC fuzzy are chosen using qualitative and quantitative analysis where the output sets are selected based on the average of the input sets as represented in Table 4.2.

Table 4.2: Fuzzy rules for fuzzy logic controller.

| $ez^{-1}$ | <b>e</b> | <b>NB</b> | <b>NM</b> | <b>NS</b> | <b>ZE</b> | <b>PS</b> | <b>PM</b> | <b>PB</b> |
|-----------|----------|-----------|-----------|-----------|-----------|-----------|-----------|-----------|
| <b>NB</b> |          | NB        | NB        | NB        | NM        | NS        | NVS       | ZE        |
| <b>NM</b> |          | NB        | NB        | NM        | NS        | NVS       | ZE        | PVS       |
| <b>NS</b> |          | NB        | NM        | NS        | NVS       | ZE        | PVS       | PS        |
| <b>ZE</b> |          | NM        | NS        | NVS       | ZE        | PVS       | PS        | PM        |
| <b>PS</b> |          | NS        | NVS       | ZE        | PVS       | PS        | PM        | PB        |
| <b>PM</b> |          | NVS       | ZE        | PVS       | PS        | PM        | PB        | PB        |
| <b>PB</b> |          | ZE        | PVS       | PS        | PM        | PB        | PB        | PB        |

Where the notations represent: NB: Negative Big, NM: Negative Medium, NS: Negative Small, NVS: Negative Very Small, ZE: Zero, PS: Positive Small, PM: Positive Medium, PB: Positive Big, and PVS: Positive Very Small.

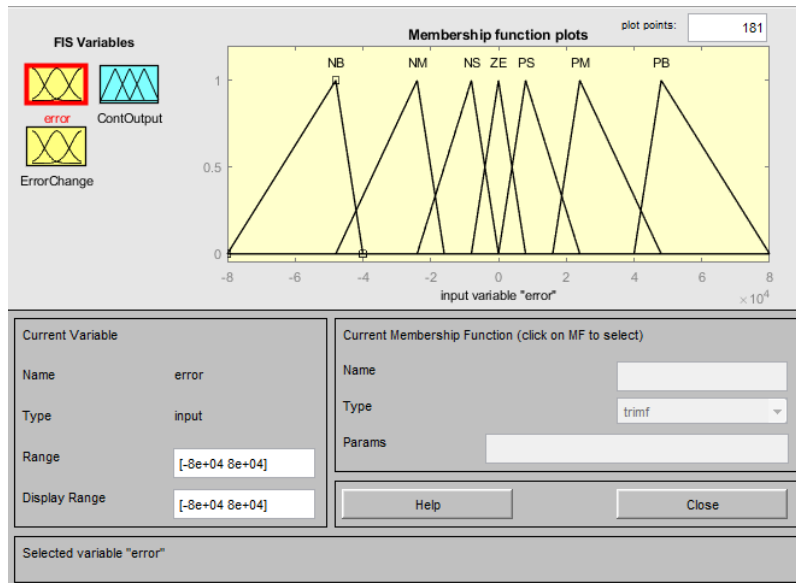


Figure 4.7: Input membership functions for fuzzy controller.

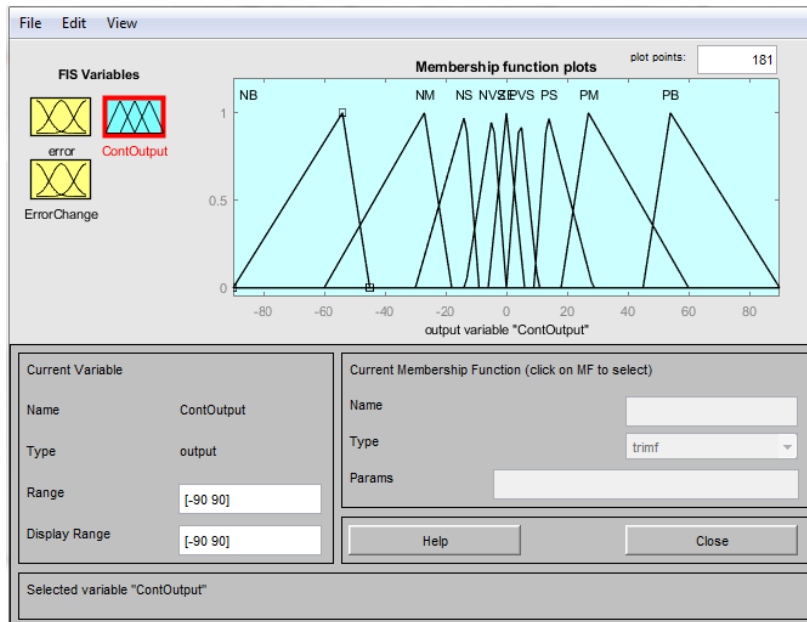


Figure 4.8: Output membership functions for fuzzy controller.

## 4.4 Fuzzy PI Control

Fuzzy PI controller is a hybrid controller that employs PI gains to create a nonlinear response [22]. In this work, suitable PI gains were selected using trail error tuning method to obtain best system response that maximizes power extraction at different wind speeds. The obtained PI gains are:  $k_p = 0.5771$  and  $k_i = 491.5995$ . Two fuzzy logic controller inputs are chosen: i) The rotor current error and ii) The one-step delayed rotor current error. The appropriate set of rules, represented in Table 4.3, was constructed using trail and error method. The columns refer to the error  $e(t)$  whereas the rows refer to delayed error signal  $ez^{-1}(t)$ . Each pair( $e(t)$ ,  $ez^{-1}(t)$ ) identifies the output level  $u(t)$ . Similar to the proposed FLC design, the Fuzzy PI membership functions of input  $e(t)$  are identical to those of  $ez^{-1}(t)$ . The membership functions are designed to satisfy the best response results. Similar to the fuzzy design, the range of both inputs is chosen to be  $[-80000 \ 80000]$  and the output range is set to  $[-90 \ 90]$  based on trail and error as exhibited in Fig.4.9 and 4.10, respectively. The design consists of five membership functions for both inputs and output. The five membership functions consists of three triangular functions and two Z-shaped membership functions (zmf). The fuzzy rules are represented in Table 4.3, where the notations representation is as follows: BN: Big Negative, N: Negative, Z: Zero, P: Positive and BP: Big Positive.

Table 4.3: Fuzzy rules for Fuzzy-PI controller.

| $ez^{-1}$ | e | <b>BN</b> | <b>N</b> | <b>Z</b> | <b>P</b> | <b>BP</b> |
|-----------|---|-----------|----------|----------|----------|-----------|
| <b>BN</b> |   | BN        | Z        | BN       | Z        | Z         |
| <b>N</b>  |   | Z         | N        | N        | Z        | Z         |
| <b>Z</b>  |   | BN        | N        | Z        | P        | BP        |
| <b>P</b>  |   | Z         | Z        | P        | P        | Z         |
| <b>BP</b> |   | Z         | Z        | BP       | Z        | BP        |

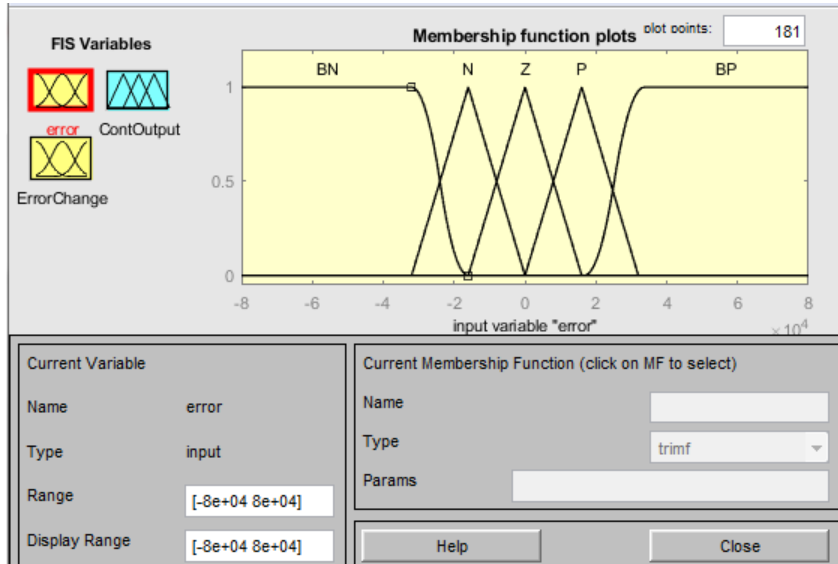


Figure 4.9: Input membership functions for fuzzy-PI controller.

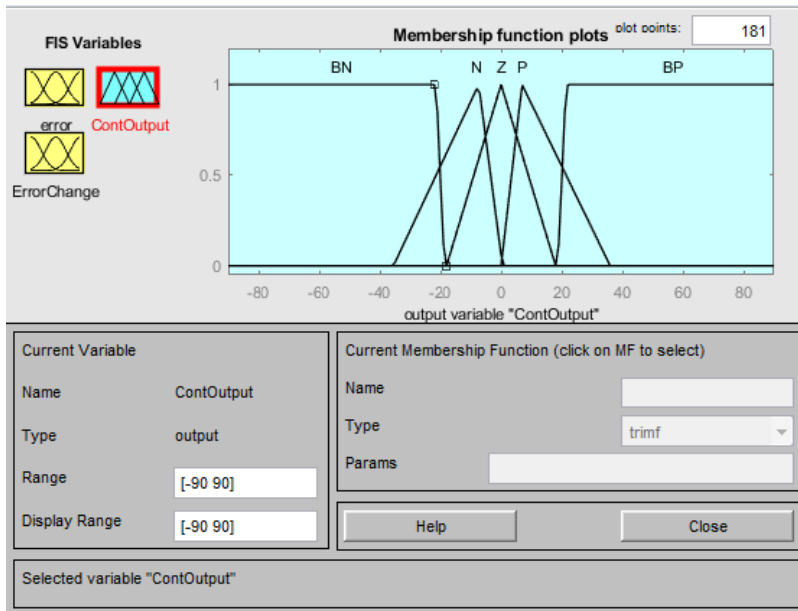


Figure 4.10: Output membership functions for fuzzy-PI controller.



# Chapter 5 : Simulation and Results

## 5.1 Model Simulation

Wind speed model along with turbine model that includes the aerodynamic, mechanical, electrical and control systems are simulated using Simulink.

### 5.1.1 Wind Speed Model Simulation

The wind speed model consists of average wind speed component, ramp component, gust component and turbulence component. The simulated wind model is represented in Fig. 5.1. According to Eq. (3.6), the transfer function of the first order filter is represented by:  $\frac{300s}{300s+1}$ .

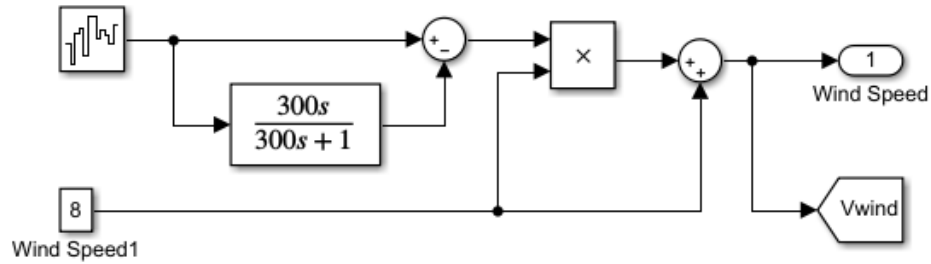


Figure 5.1: Wind speed model simulation with average speed of 8m/s.

### 5.1.2 Aerodynamic Model Simulation

The aerodynamic model, represented in Fig. 5.2, is designed to evaluate the aerodynamic torque of the turbine shaft  $T_{ae}$  according to Eq. 5.1 [43]:

$$T_{ae} = \frac{\pi}{2\lambda} \rho R^3 v_{eq}^2 C_p(\theta_{pitch}, \lambda) \quad (5.1)$$

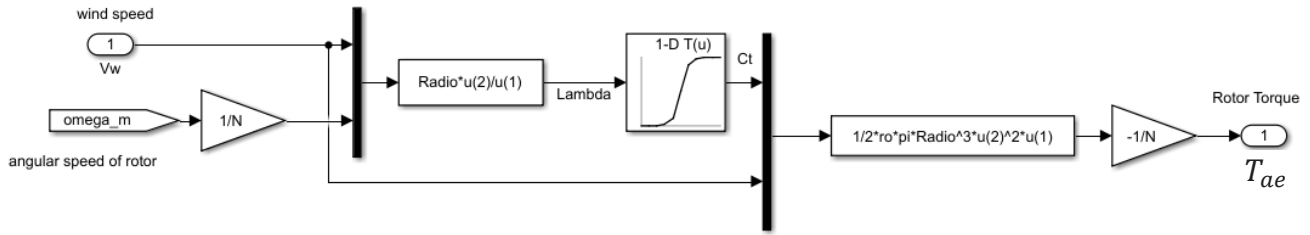


Figure 5.2: Aerodynamic system simulation of a WT.

### 5.1.3 Electrical Model Simulation

Fig. 5.3 represents the electrical system model which includes the DFIG that has its rotor connected to the rotor side convertor from the right, and its stator to the grid from the left. The grid side converter is replaced by a DC voltage source for simplicity.

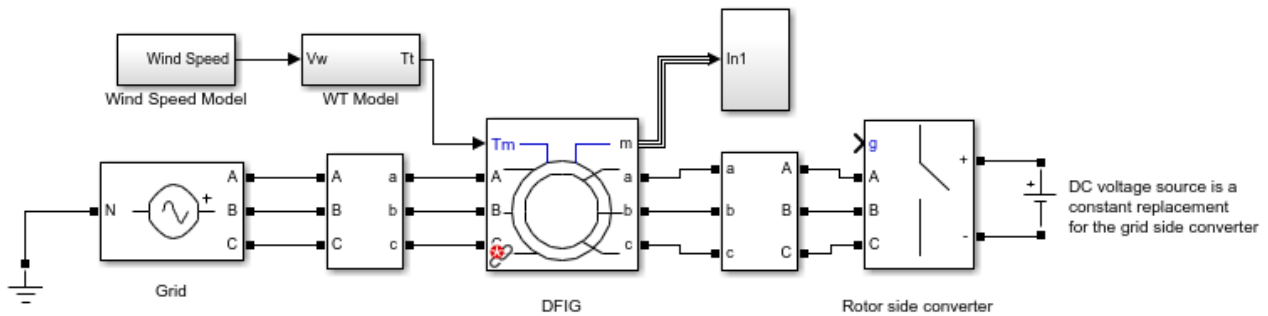


Figure 5.3: Electrical system simulation of a DFIG wind turbine.

### 5.1.4 Control System Simulation

In this work, an indirect speed control is designed to force the aerodynamic torque  $T_{ae}$  to follow the maximum power curve in response to wind variations. Moreover, a vector controller for current loops is designed to control the rotor side converter. Fig. 5.4 shows the control system of DFIG wind turbine while Fig. 5.5 exhibits the overall Simulink design. The design consists of a DFIG that is equipped with a wound rotor induction generator that has a voltage source converter connected to the slip-rings of the rotor the grid is directly coupled to the stator winding while the power converter is connected to the rotor winding.

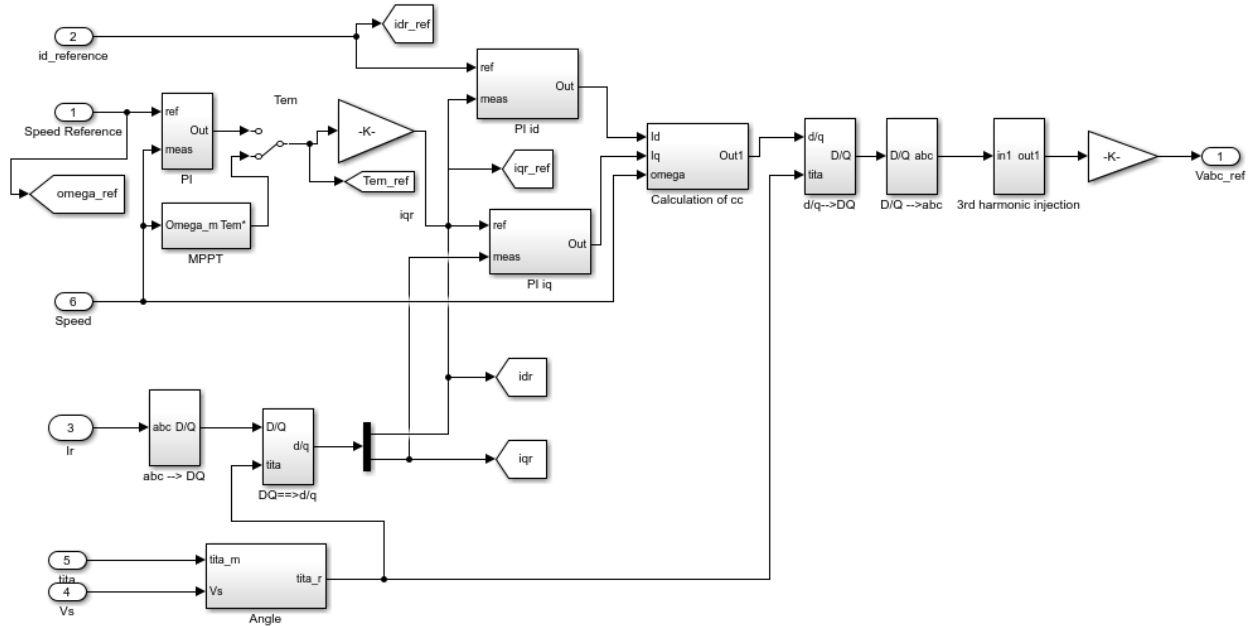


Figure 5.4: Control system simulation of a DFIG WT.

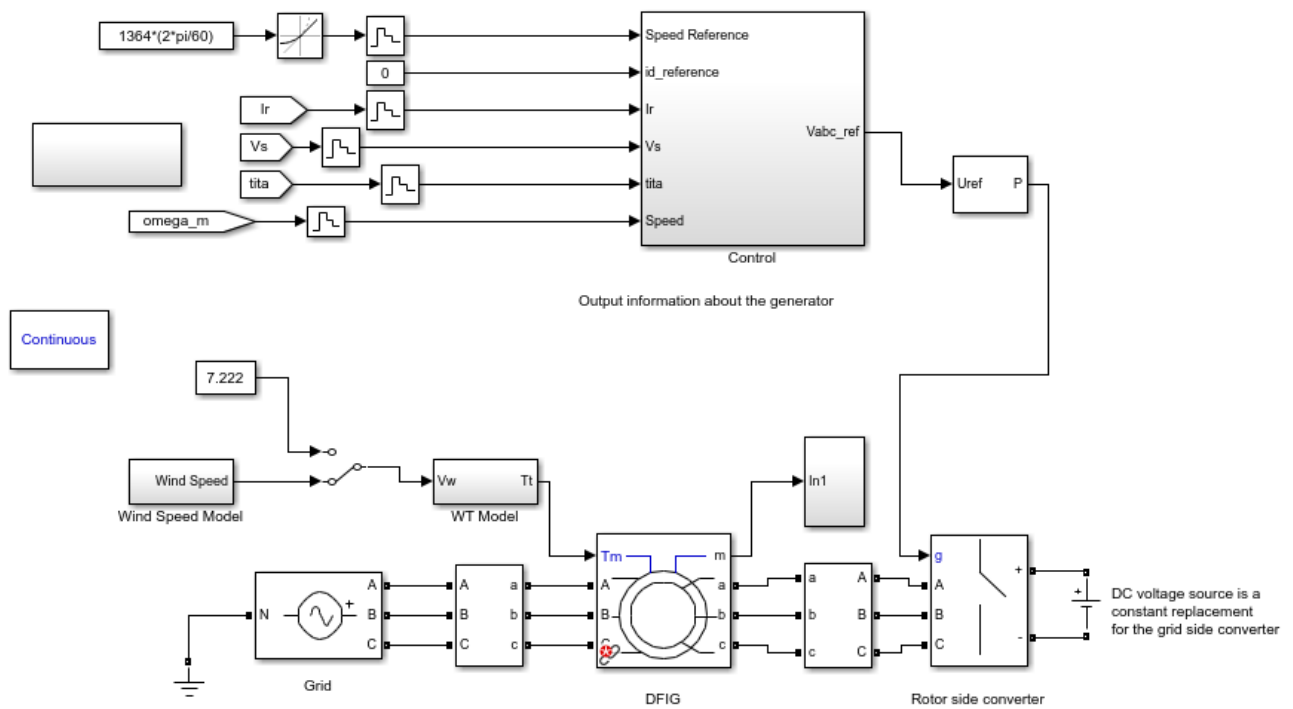


Figure 5.5: Overall WT dynamic model design in Simulink.

## 5.2 Steady state analysis

Table 5.1 shows the 2 MW DFIG parameters that are subject to the manufacturer design of the machine [43]. These parameters are used to evaluate the steady state magnitudes of the parameters shown in Table 5.2, with  $i_{dr} = 0$ .

Table 5.1: 2 MW DFIG characteristics

|  |   |
|--|---|
| Stator frequency (Hz)                      | $f=50$                                  |
| Rated stator power (W)                     | $P_s=2 \times 10^6$                     |
| Rated rotational speed (rev/min)           | $n=1500$                                |
| Rated stator voltage (V)                   | $V_s=690$                               |
| Rated stator current (A)                   | $I_s=1760$                              |
| Rated torque (N.m)                         | $T_{em}=12732$                          |
| Pole pair                                  | $p=2$                                   |
| Stator/rotor turns ratio                   | $u=1/3$                                 |
| Rated rotor voltage (V)                    | $V_r=2070$                              |
| Maximum slip                               | $s_{max}=1/3$                           |
| Rated rotor voltage referred to stator (V) | $V_{r\_stator}=(V_r*s_{max})*u$         |
| Stator resistance (ohm)                    | $R_s=2.6 \times 10^{-3}$                |
| Leakage inductance (stator/rotor) (H)      | $L_{si}=0.087 \times 10^{-3}$           |
| Magnetizing inductance (L)                 | $L_m=2.5 \times 10^{-3}$                |
| Rotor resistance referred to stator (ohm)  | $R_r=2.9 \times 10^{-3}$                |
| Stator inductance (H)                      | $L_s=L_m+L_{si}$                        |
| Rotor inductance (H)                       | $L_r=L_m+L_{si}$                        |
| DC bus voltage referred to stator (V)      | $V_{bus}=V_{r\_stator} \times \sqrt{2}$ |

The DFIG rotor speed was set to be in the range between 900 and 1800 revolutions per minute, and accordingly the other parameters are calculated. Fig. 5.6 exhibits the steady state characteristics of a 2MW DFIG. It is noted that the electromagnetic rotor torque  $T_{em}$  is negative which indicated that the Doubly Fed Induction Machine (DFIM) is functioning as a generator. The total mechanical power  $P_t$  of the shaft represents the product of the electromagnetic torque and the rotor speed. The stator active power  $P_s$  is found to be much bigger than the rotor active power  $P_r$ . For example, the maximum stator active power is about 2 MW while the maximum rotor active power is around 400 kW. Note that the negative and positive values of the active power represent the rotational speed direction of the rotor. Both the stator and rotor currents increase as the rotational speed increases. The stator is directly connected to the grid; hence, its voltage is always around 690 V according to the Mitsubishi design. On the other hand, the rotor voltage depends on the rotational speed where the minimum rotor voltage

occurs at the synchronous speed. The stator reactive power  $Q_s$  is much larger than the rotor reactive power  $Q_r$ . Finally, the efficiency of the machine particular (the mechanical power in the shaft) to motor or generator operation is considered almost constant through all rotational speed values [42].

Table 5.2: Equations of steady state magnitudes when  $i_{dr}=0$  [42].

|                 |  |  |   |  |
|-----------------|--|--|---|--|
| Stator Flux     | $ \vec{\psi}_s  = \sqrt{\frac{-B \pm \sqrt{B^2 - 4AC}}{2A}}$ | $C = \left(\frac{2}{3} \frac{R_s T_{em}}{p L_m}\right)^2$                                    | $B = \frac{4}{3} \frac{R_s T_{em} \omega_s}{p} -  v_s ^2$ | $A = \left(\frac{R_s}{L_s}\right)^2 + \omega_s^2$                  |
| Rotor Currents  | $i_{dr} = 0$   | $i_{qr} = \frac{T_{em}}{-\frac{3}{2} p \frac{L_m}{L_s}  \vec{\psi}_s }$                      | $ \vec{i}_r ^2 = i_{dr}^2 + i_{qr}^2$                     | $\theta_{i_s} = a \tan\left(\frac{i_{qs}}{i_{ds}}\right)$          |
| Stator Currents | $i_{dr} = \frac{ \vec{\psi}_s }{L_s}$                        | $i_{qs} = -\frac{L_m}{L_s} i_{qr}$   | $ \vec{i}_s ^2 = i_{ds}^2 + i_{qs}^2$                     | $\theta_{i_s} = a \tan\left(\frac{i_{qs}}{i_{ds}}\right)$          |
| Stator Voltage  | $v_{ds} = R_s i_{ds}$  | $v_{qs} = R_s i_{qs} + \omega_s  \vec{\psi}_s $  | $ \vec{v}_s ^2 = v_{ds}^2 + v_{qs}^2$                     | $\theta_{v_s} = a \tan\left(\frac{v_{qs}}{v_{ds}}\right)$          |
| Slip            | $\omega_r = \omega_s - \omega_m$                             |  | $s = \omega_r / \omega_s$                                 |  |
| Rotor Voltages  | $v_{dr} = R_r i_{dr} - \omega_r \sigma L_r i_{qr}$           | $v_{qr} = R_r i_{qr} + \omega_r \sigma L_r i_{dr} + \omega_r \frac{L_m}{L_s}  \vec{\psi}_s $ | $ \vec{v}_r ^2 = v_{dr}^2 + v_{qr}^2$                     | $\theta_{v_r} = a \tan\left(\frac{v_{qr}}{v_{dr}}\right)$          |
| Rotor Fluxes    | $\psi_{dr} = L_m i_{ds} + L_r i_{dr}$                        | $\psi_{qr} = L_m i_{qs} + L_r i_{qr}$  | $ \vec{\psi}_r ^2 = \psi_{dr}^2 + \psi_{qr}^2$            | $\theta_{\psi_r} = a \tan\left(\frac{\psi_{qr}}{\psi_{dr}}\right)$ |
| Active Powers   | $P_m = T_{em} \frac{\omega_m}{p}$                            | $P_s = \frac{3}{2} (v_{ds} i_{ds} + v_{qs} i_{qs})$  | $P_r = \frac{3}{2} (v_{dr} i_{dr} + v_{qr} i_{qr})$       |  |
| Reactive Powers | $Q_s = \frac{3}{2} (v_{qs} i_{ds} - v_{ds} i_{qs})$          | $PF_s = \cos(a \tan(Q_s/P_s))$   | $Q_r = \frac{3}{2} (v_{qr} i_{dr} - v_{dr} i_{qr})$       | $PF_r = \cos(a \tan(Q_r/P_r))$                                     |
| Effeciency      | $\eta = \frac{P_m}{P_s + P_r}$ if $P_m > 0$                  |  |   |  |

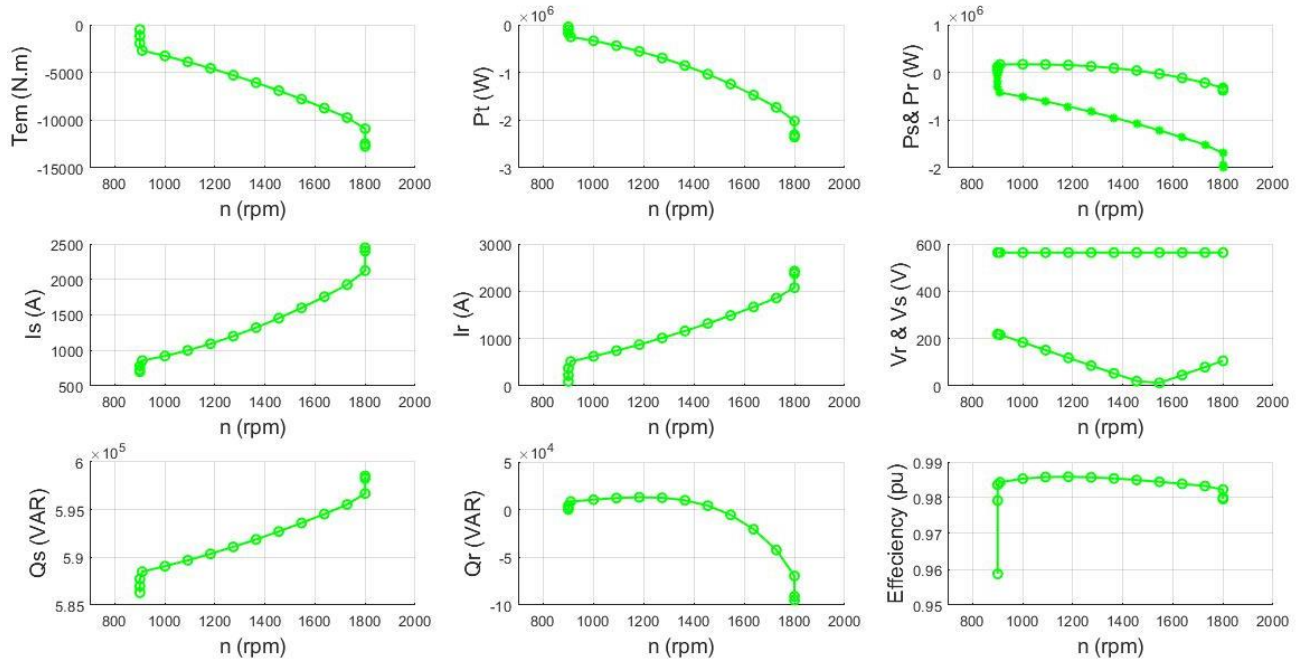


Figure 5.6: Steady state magnitudes of a 2 MW DFIG.

The steady state performance of a 2 MW DFIG presented in Fig. 5.6 is studied to evaluate the designed system at rotational speed of 1364 rev/min and the corresponding electromagnetic torque of -6050 Nm. In other words, the designed system is tested at DFIG rotational speed of 1364 rev/min and the values of  $I_s$ ,  $I_r$  and  $V_r$  are compared to the ones represented in Fig 5.6 at rotational speed of 1364 rev/min. the objective of this step is to have simulation values of  $I_s$ ,  $I_r$  and  $V_r$  equal to the steady state values in order to verify our design.

### 5.3 Performance analysis

In this section, the simulation results of the DFIG-Based wind turbine system using the three proposed controllers are analyzed and discussed.

#### 5.3.1 Simulation results for different wind speeds using PI controller

Fig. 5.7 represents the steady state analysis of the simulated system at rotational speed of 1364 rev/min. It is noticed that the steady state values of speed, torque, rotor current, stator current and rotor voltage match the values given in Fig. 5.6. The rotor speed is 142.8 rad/s which is equivalent to 1364 rev/min

$\left(\frac{1364 \frac{rev}{min} \times 2\pi \frac{rad}{rev}}{60 \frac{min}{s}} = 142.8 \frac{rad}{s}\right)$  that was set as reference speed. The electromagnetic torque at the steady

state is  $-6047$  (N.m) that is very close to the reference value. Note that the rotor current in the  $d$  direction is forced to go to  $0$  A in order to make it easier to control the current in the  $q$  direction which reaches the value of  $I_{qr\_ref}$  at steady state, which corresponds to the peak value of the three-phase rotor current  $I_r$  [42]. It is also observed that the  $i_{qr}$  has the same value of  $I_r$  in Fig. 5.6. The peak of  $I_s$  in Fig. 5.7 is equivalent to the  $I_s$  value of Fig. 5.6. Hence, it is concluded from the obtained results that the system is working properly and following the manufacturer design. Finally the values of  $v_{qr}$  and  $v_{dr}$  are validated using Eq. 5.2,

$$\sqrt{v_{qr}^2 + v_{dr}^2} = V_r = \sqrt{-3.699^2 + 50.04^2} = 50.1675 \text{ V.} \quad (5.2)$$

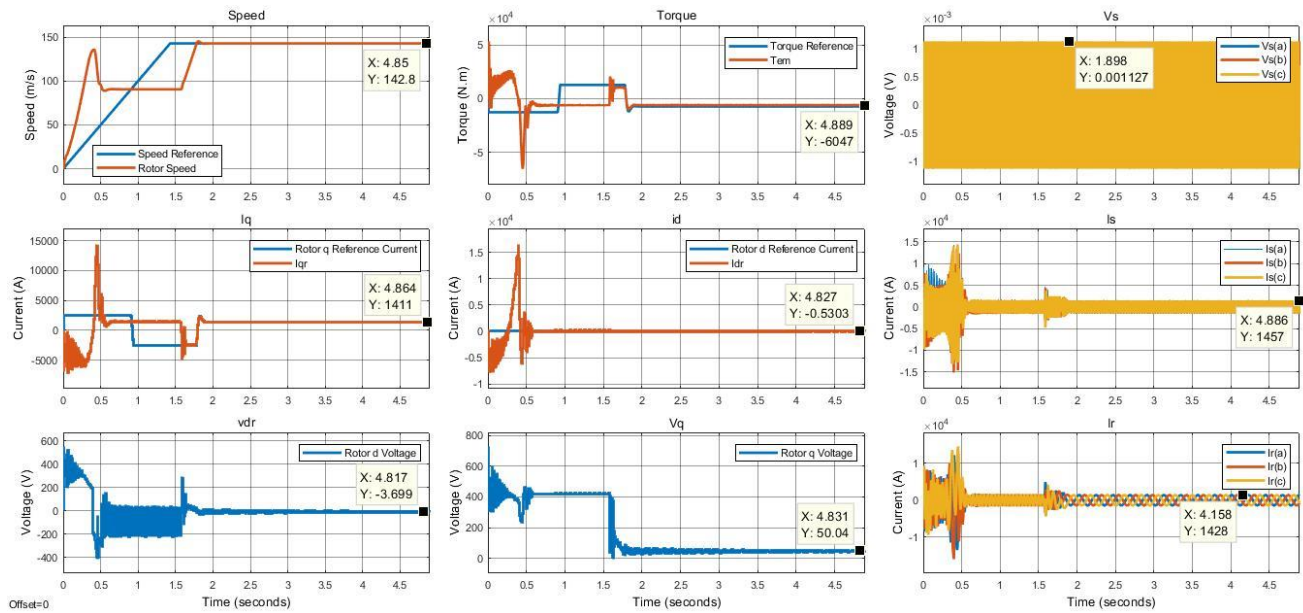


Figure 5.7: Steady state response of the simulated system with rotor speed of 142.8 rad/sec.

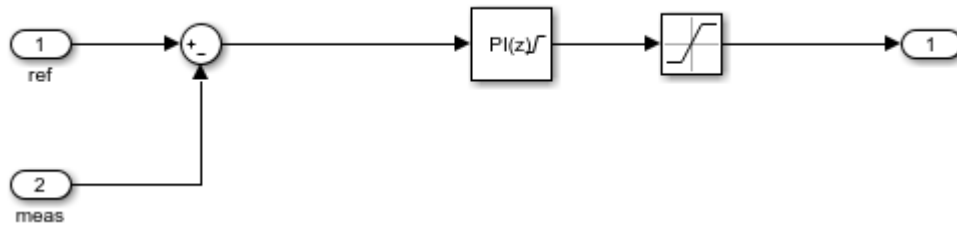


Figure 5.8: PI controller design of the DFIG wind turbine.

Fig. 5.8 represents the designed PI controller using Simulink. Table 5.4 represents the steady state values (rotor speed and electromagnetic torque) corresponding to different wind speeds.

Table 5.3: Design simulation with certain wind speed values and their corresponding power and steady state magnitudes of the rotor speed and the electromagnetic torque using PI controller.

| Wind Speed (m/s) | Power (MW)             | Rotor Speed | Electromagnetic Torque |
|------------------|------------------------|-------------|------------------------|
| 7.2              | $132.5 * 4196 = 0.56$  |             |                        |
| 10               | $183.4 * 8151 = 1.494$ |             |                        |
| 13.3             | $217.5 * 1034 = 2.248$ |             |                        |

The simulation results follow the design characteristics as long as the wind speed does not exceed 12.22 m/s. For increasing wind speeds, the pitch control will take place in order to reduce the aerodynamic performance of the turbine and limit the power extraction. In our simulation, the pitch control was not designed which justifies the difference between the reference and obtained power values. In other words, the designed system performs as required as long as the wind speed is below 12.22 m/s. The next step is integrating wind speed model with the wind turbine. The average wind speed component is selected to be 8 m/s while the ramp, gust and turbulence components are generated automatically by



the system. Fig. 5.9 exhibits the wind speed variations and Fig. 5.10 represents the main DFIG parameters that correspond to the selected wind speed. Note that the power generated by the wind turbine is 0.769 MW that corresponds, according to Fig. 4.4, to wind speed value of 8 m/s, which is, in this case, the average speed component.

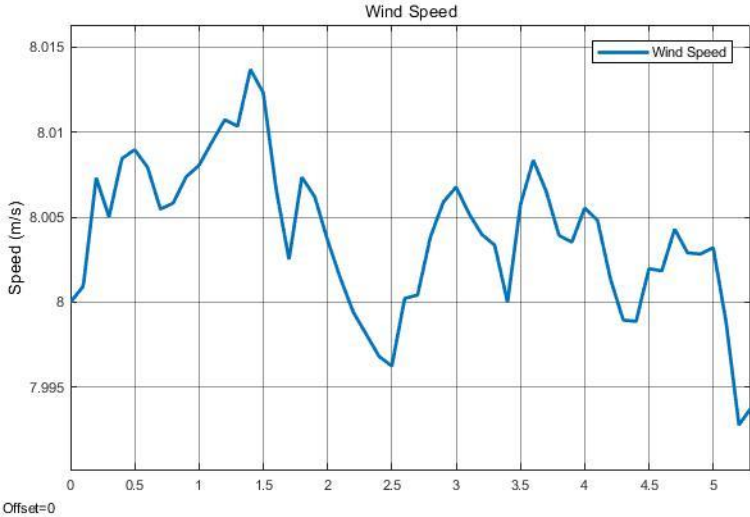


Figure 5.9: Wind speed signal

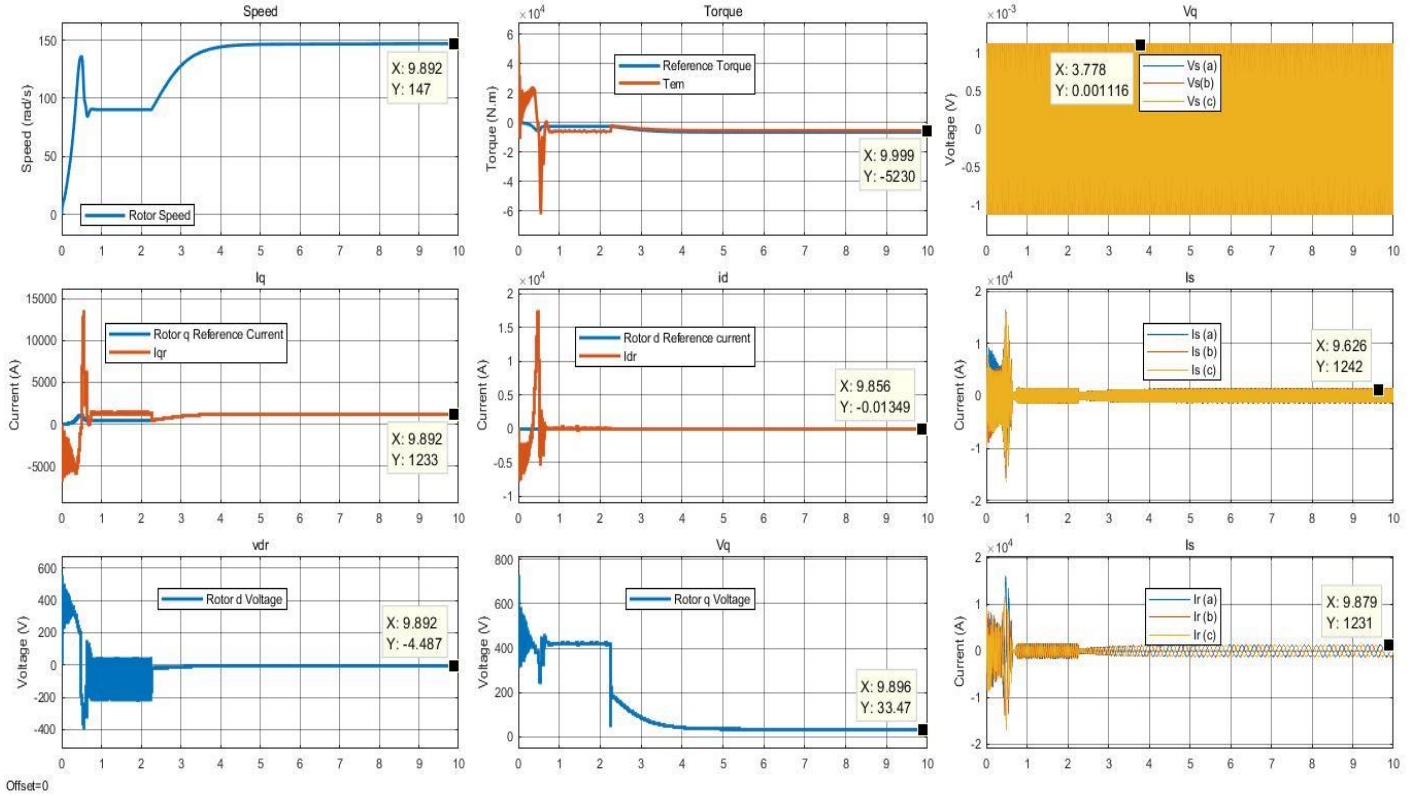


Figure 5.10: Steady state simulation for DFIG with PI controller at average wind speed component of 8 m/s.

The analysis of peak overshoot/undershoot, steady state error, and settling time of the rotor speed, electromagnetic torque,  $i_q$  and  $i_d$  components of the rotor current are presented in Table 5.4.

Table 5.4: Steady state analysis for DFIG wind turbine with PI controller.

|                              | Rotor Speed   | Torque     | $i_{dr}$ | $i_{qr}$ |
|------------------------------|---------------|------------|----------|----------|
| <b>Peak Overshoot</b>        | 136.5 rad/sec | 53800      | 17520 A  | 13630 A  |
| <b>Peak Undershoot</b>       | -             | -62300 N.m | -7840    | -6881    |
| <b>Steady state error</b>    | -             | -          | 0.01349  | 0.0017   |
| <b>Settling time (5%)(s)</b> | 3.463         | 3.711      | 8.706    | 3.9      |

### 5.3.2 Simulation results for different wind speeds using Fuzzy controller

As observed from section 5.3, the PI controllers for the  $i_{qr}$  and  $i_{dr}$  could not satisfy the required system performance as the settling time of the  $i_{dr}$  component is considered high as well as the overshoot/undershoot for all parameters. Therefore, a modern efficient controller, i.e. fuzzy logic controller, is introduced to enhance the output response. The designed fuzzy logic controller,

represented in Fig. 5.11, is tested at three different wind speed values to assure that it meets the 2 MW DFIG specifications.

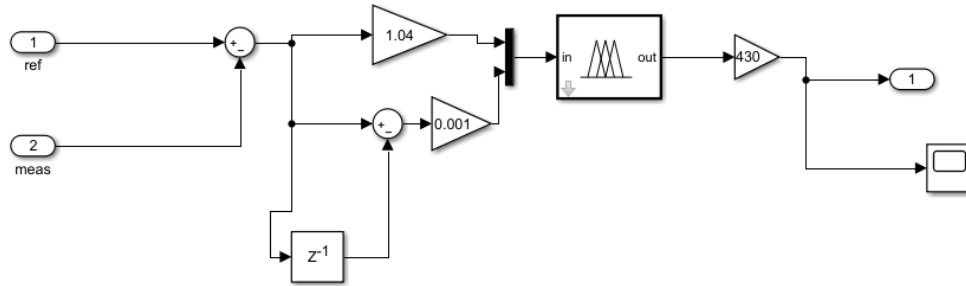


Figure 5.11: Fuzzy logic controller for the rotor current components.

It is observed from Table 5.5 that the power values matches the ones represented in Table 4.1 for wind speeds of 7.2 m/s and 10 m/s. Hence, the controlled system behaves as required at speeds values below 12.22 m/s. Similar to the PI controller analysis, the 13.3 m/s requires integrating pitch controller to obtain the required power value. The complete designed system is simulated at wind speed of 8 m/s, shown in Fig 5.12, to observe the overshoot/undershoot, steady state error and settling time as represented in Table 5.6.

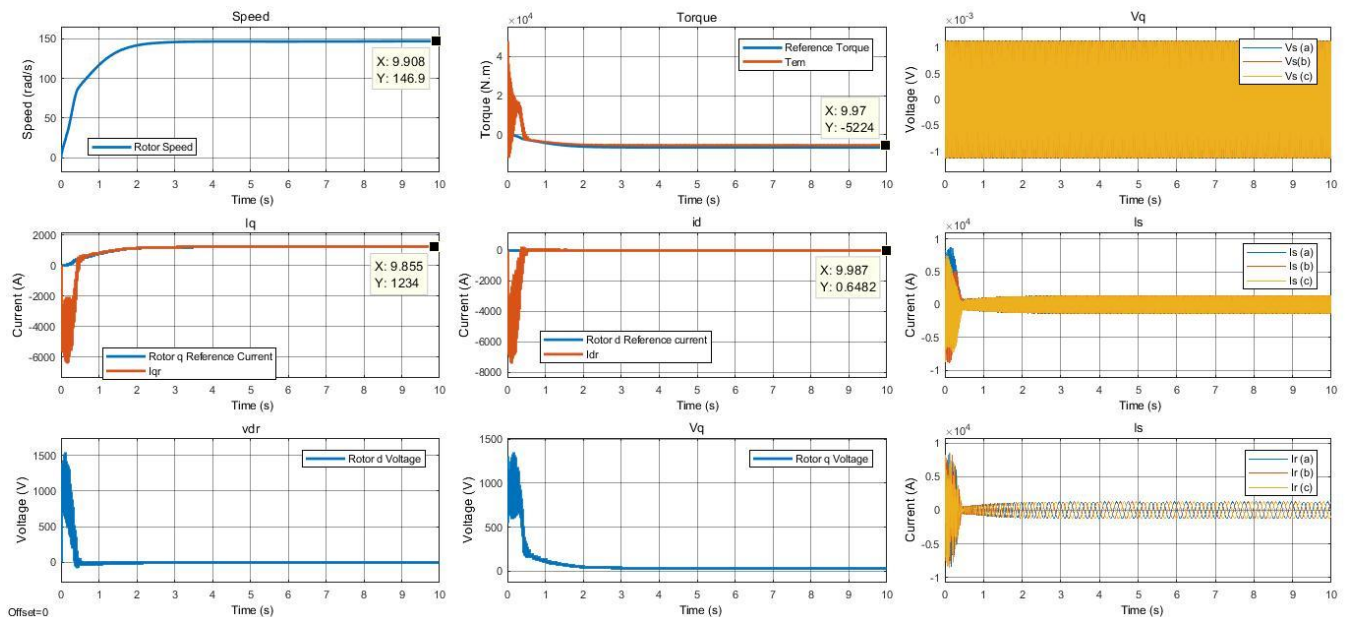


Figure 5.12: Steady state simulation for DFIG with fuzzy logic controller at average wind speed component of 8 m/s.

Table 5.5: Design simulation with certain wind speed values and their corresponding power and steady state magnitudes of the rotor speed and the electromagnetic torque using fuzzy logic controller.

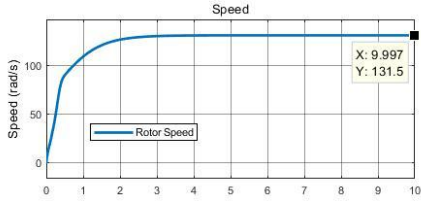
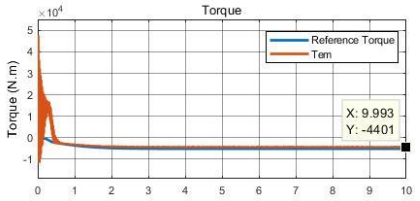
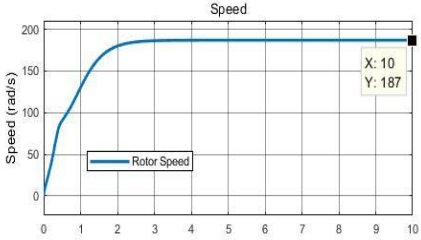
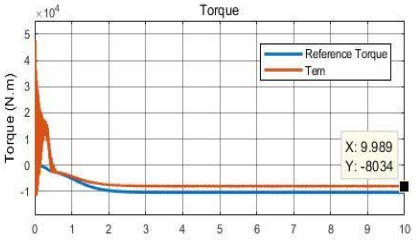
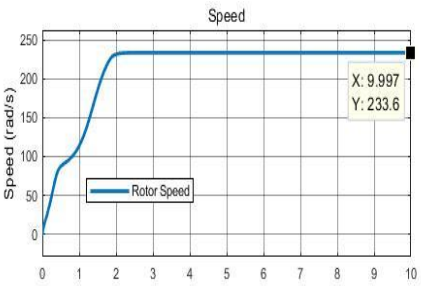
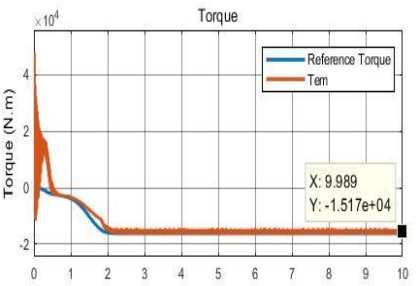
| Wind Speed (m/s) | Power (MW)                 | Rotor Speed   | Electromagnetic Torque   |
|------------------|----------------------------|---|--|
| 7.2              | $131.5 \times 4401 = 0.57$ |   |   |
| 10               | $187 \times 8034 = 1.502$  |   |   |
| 13.3             | $233.6 \times 1517 = 3.54$ |  |  |

Table 5.6: Steady state analysis for DFIG wind turbine with fuzzy logic controller.

|                              | Rotor Speed | Torque     | <i>idr</i> | <i>iqr</i> |
|------------------------------|-------------|------------|------------|------------|
| <b>Peak Overshoot</b>        | -           | 47510 N.m  | 328.4 A    | -          |
| <b>Peak Undershoot</b>       | -           | -11900 N.m | -7469 A    | -6485 A    |
| <b>Steady state error</b>    | -           | -          | 0.608      | 2          |
| <b>Settling time (5%)(s)</b> | 1.789       | 2.295      | 7.242      | 2.064      |

### 5.3.3 Comparison between Fuzzy Controller and PI controller

By comparing the corresponding parameters in Table 5.4 and Table 5.6, it is observed that the DFIG wind turbine response with fuzzy controller shows enhancements in terms of the peak overshoot, peak

undershoot and settling time when compared to system with PI controller. However, the steady state error values are higher for the fuzzy logic controller. Fig. 5.13 represents fewer oscillations for the fuzzy design compared to the PI design.

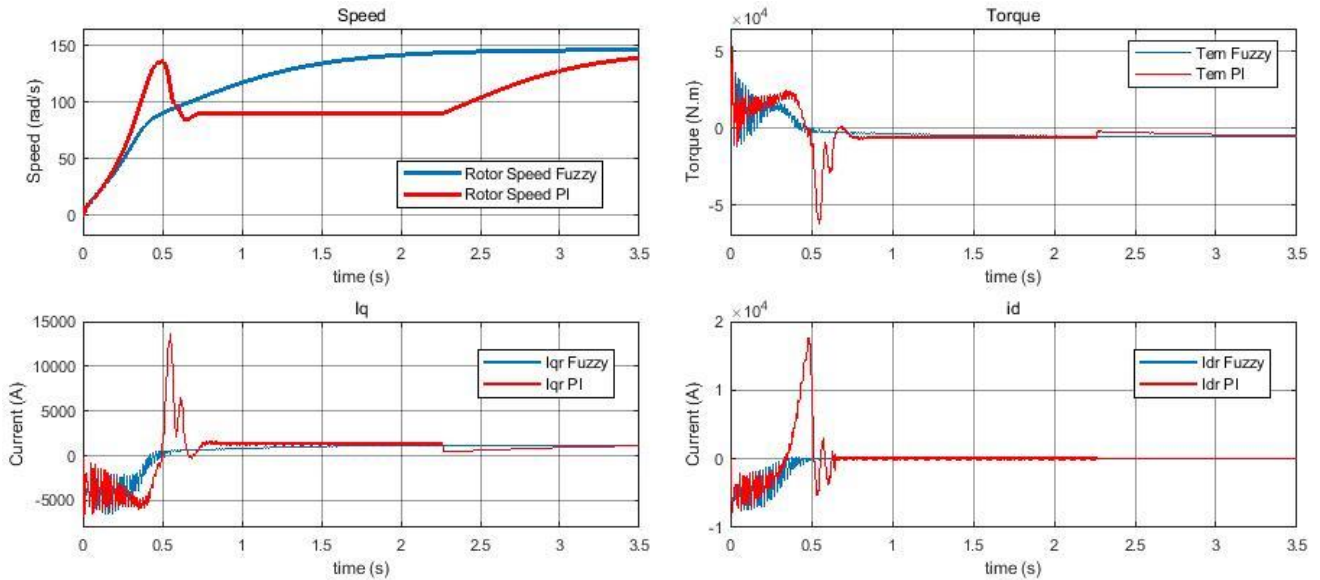


Figure 5.13: Steady state simulation for DFIG with fuzzy logic controller and PI controller at average wind speed component of 8 m/s.

### 5.3.4 Simulation results for different wind speeds using fuzzy-PI controller

As observed from section 5.3.2, the fuzzy logic controllers for the  $i_{qr}$  and  $i_{dr}$  could not satisfy the required system performance in terms of the high steady state error values. Hence, as an enhancement, a fuzzy-PI controller is designed as represented in Fig. 5.14.

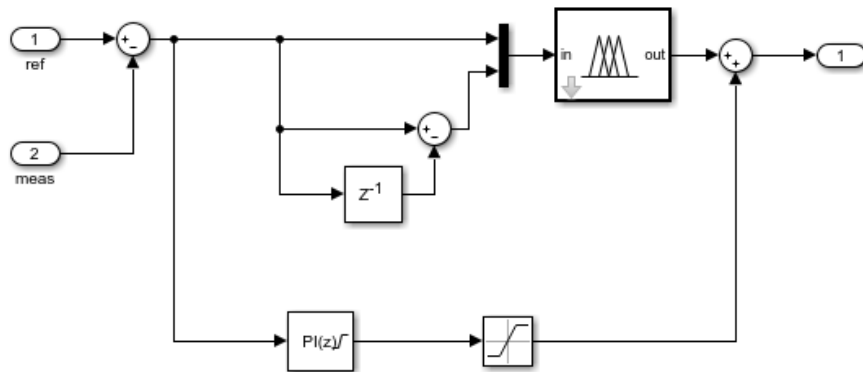
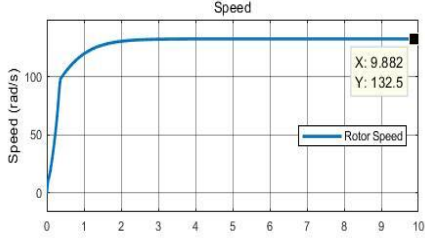
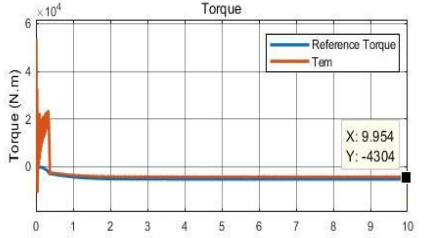
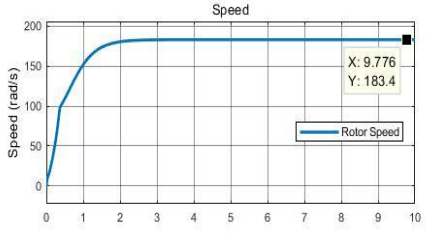
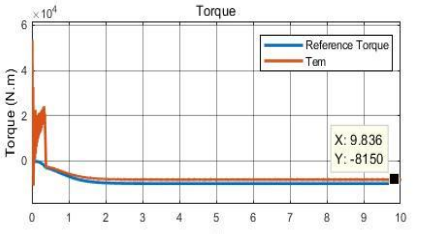
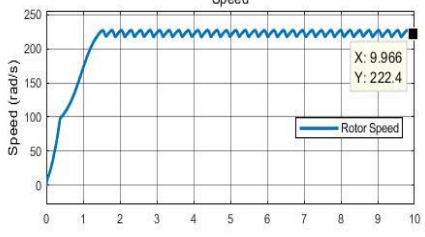
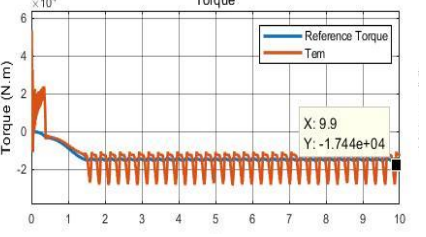


Figure 5.14: Fuzzy-PI controller design for rotor current components.

The system with the fuzzy-PI controller is simulated using the algorithm in Fig. 5.14 at three different wind speeds. Table 5.7 shows the extracted power which is equivalent to the product of the rotor speed and the electromagnetic torque for different wind speed values.

Table 5.7: Design simulation with certain wind speed values and their corresponding power and steady state magnitudes of the rotor speed and the electromagnetic torque using fuzzy-PI controller.

| Wind Speed (m/s) | Power (MW)              | Rotor Speed  | Electromagnetic Torque  |
|------------------|-------------------------|--|---|
| 7.2              | $132.5 * 4304 = 0.57$   |    |    |
| 10               | $1873.4 * 8150 = 1.502$ |   |   |
| 13.3             | $222.4 * 17440 = 3.87$  |  |  |

It can be concluded from Table 5.7 that the obtained power values validates the designed system as they matched the ones represented in Table 4.1 for wind speed of 7.2 m/s and 10 m/s. However, similar to the previous cases, the wind speed of 13.3 m/s forces the DFIG wind turbine with fuzzy-PI controller to have more oscillations in the rotor speed and current values that result in having unrealistic power values. The performance of the fuzzy-PI controller system is shown in Fig. 5.15 and summarized in Table 5.8. The steady-state characteristics of rotor speed, torque,  $i_{dr}$  and  $i_{qr}$  represented in Table 5.8

are evaluated at wind speed of 8 m/s. Note that the rotor speed and torque do not have steady state error as they do not have a reference value to be compared with.

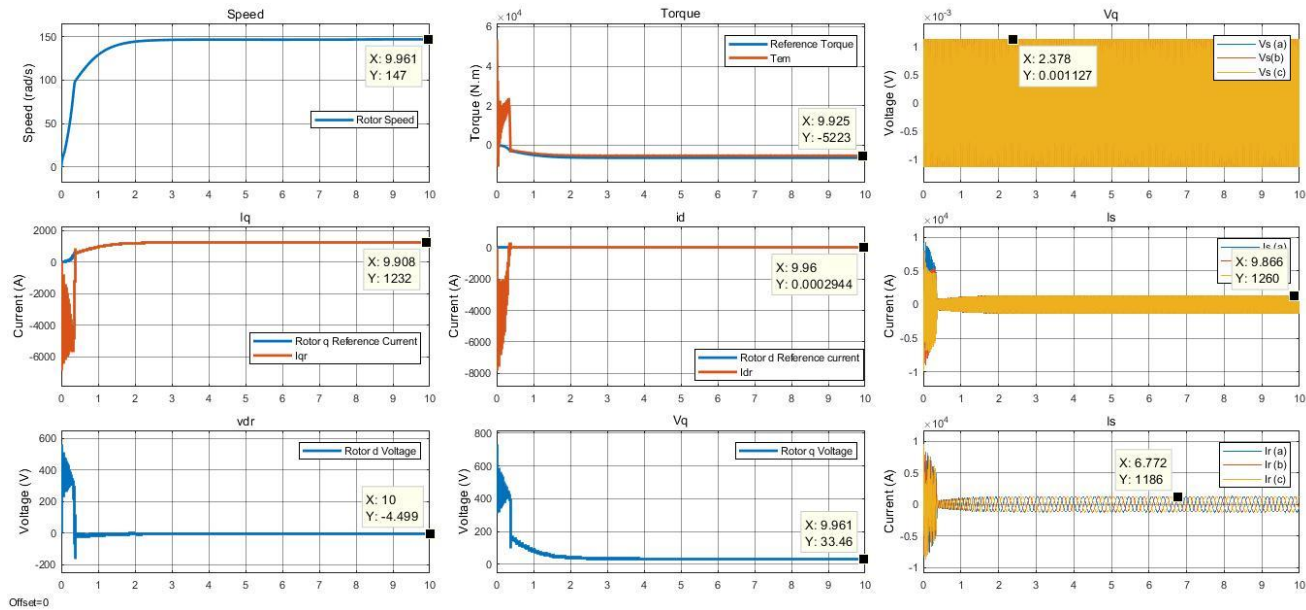


Figure 5.15: Steady state simulation for DFIG with fuzzy-PI controller at average wind speed component of 8 m/s.

Table 5.8: Steady state analysis for DFIG wind turbine with fuzzy-PI controller.

|                              | <b>Rotor Speed</b> | <b>Torque</b> | <b><i>idr</i></b> | <b><i>iqr</i></b> |
|------------------------------|--------------------|---------------|-------------------|-------------------|
| <b>Peak Overshoot</b>        | -                  | 52310         | 333.1             | 839.5             |
| <b>Peak Undershoot</b>       | -                  | -10900        | -7826             | -6868             |
| <b>Steady state error</b>    | -                  | -             | 0.0002944         | 0.001             |
| <b>Settling time (5%)(s)</b> | 1.561              | 2.012         | 5.511             | 1.703             |

### 5.3.5 Comparison between the three proposed controllers

By comparing the performance values in Table 5.6 and Table 5.8, it is observed that although the peak overshoot and undershoot values of the fuzzy-PI design response are increased by a relatively small amount, the DFIG wind turbine response with fuzzy-PI controller exhibits enhancements in terms of the settling time and steady state error. The increase in overshoot/undershoot values occurs in a very short period of time which makes it acceptable for the power system. Moreover, protection equipment such as circuit breakers and resistor banks can minimize the effect of the overshoot/undershoot on the



designed system. Fig. 5.16 represents fewer oscillations for the fuzzy-PI design and shows how the response achieves the steady state value faster than both PI controller and FLC. Fig. 5.17 represents the extracted power by the simulated wind turbine system, using the proposed control schemes, with wind speed values between 7 m/s and nominal speed (11 m/s), at the 3<sup>rd</sup> second of the simulation time. The conventional PI controlled systems exhibit degradation in the performance when compared to the other controllers. The low power extraction of the PI controller at simulation time  $t_{sim} = 3s$  is due to its long settling time  $t_{st} = 4.05s$ . On the contrary, FLC and Fuzzy PI schemes obtain higher power extraction during the whole studied range of wind speeds at  $t_{sim} = 3s$  and achieve the rated power (2MW) when the average wind speed is at its nominal value  $v_{aw} = 11$  m/s. This indicates that the settling time of extracted power is reduced as the wind speed goes higher. However, it is important to mention that for wind speeds higher than 11 m/s, the extracted power maintains 2MW. Fig. 5.18 shows a comparison between the three proposed controllers in terms of extracted power response through the first five seconds of simulation at  $v_{aw} = 11$  m/s. The Fuzzy PI controller is more efficient than other controllers as it has the lowest settling time  $t_{st} = 2.1s$ , while the PI and FLC settling times are  $t_{st} = 3.9s$  and  $t_{st} = 2.8s$  respectively. Although the Fuzzy PI overshoot is higher than the FLC overshoot, the wind turbine system is isolated from the grid until it complies with the grid requirements such as phase, frequency and voltage. Hence, the Fuzzy PI scheme demonstrates better dynamic performance by requiring smaller time to synchronize the system to the grid and achieve higher power extraction.

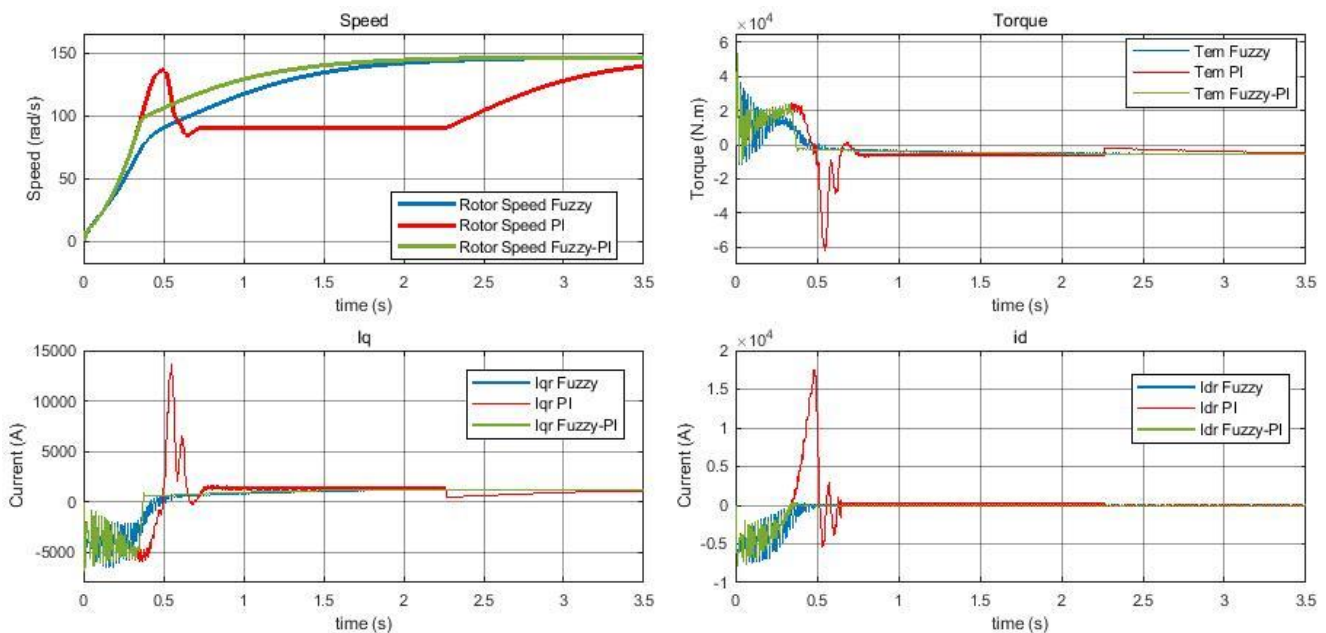


Figure 5.16: Steady state simulation for DFIG with PI controller, fuzzy logic controller, and fuzzy-PI controller at average wind speed component of 8 m/s.



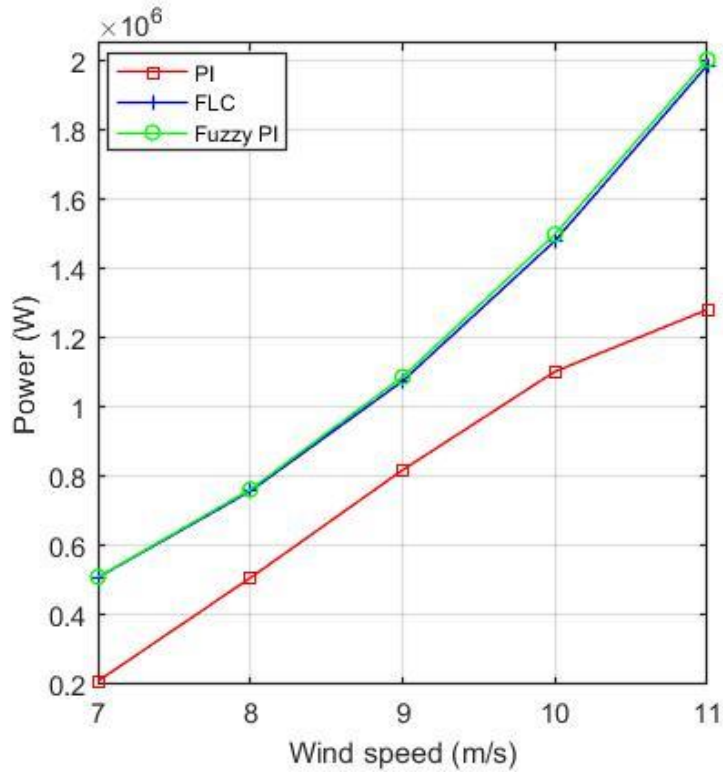


Figure 5.17: Extracted power using proposed control schemes with respect to different wind speed values.

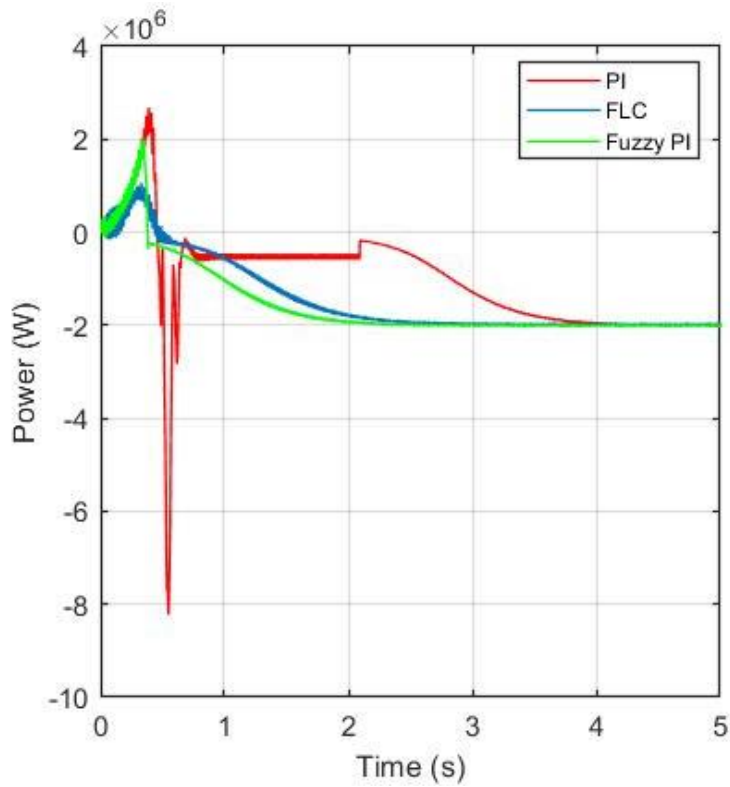


Figure 5.18: Extracted power by DFIG using PI, FLC and Fuzzy PI schemes at  $v_{ow} = 11$  m/s.

## Chapter 6 : Conclusion and Future Work

In this thesis, a 2 MW DFIG wind turbine controller designs of types PI, fuzzy logic, and fuzzy-PI are used to enhance the performance of the DFIG wind turbines. The studied model consists of a single two-mass wind turbine that is connected directly to the power system. It is assumed that the wind turbine has a general model consisting of electrical, aerodynamic, mechanical, electrical, and control system models. Wind speed model along with the turbine model are developed and analyzed using Simulink.

An indirect speed controller is designed to force the aerodynamic torque  $T_{ae}$  to follow the maximum power curve in response to wind variations, while a vector controller for current loops is designed to control the rotor side converter. PI controller was designed to control rotor current components. The gain parameters of the PI controller coefficients,  $k_p$  and  $k_i$  were tuned until the desired performance values were obtained. However, the PI design could not satisfy the required system performance as the settling time of the  $i_{dr}$  component is considered high as well as the overshoot/undershoot for all parameters. Therefore, a modern efficient controller, namely fuzzy logic based controller was introduced. Fuzzy controller showed performance enhancements in terms of the system parameters peak overshoot, peak undershoot and settling time compared to system with PI controller. However, the system parameters steady state error values are higher for the fuzzy logic controller. Finally, a fuzzy-PI controller was proposed to further enhance the system performance. Although the peak overshoot and undershoot values of the fuzzy-PI design response are increased by a relatively small amount, the DFIG wind turbine response with fuzzy-PI controller exhibits enhancements in terms of the settling time and steady state error. The steady state values of certain parameters of the DFIG wind turbine were evaluated after designing each controller, to assure that the simulation results follow the design characteristics.

As a future work, pitch control can be used to overcome any oscillations in the rotor speed of the DFIG for wind speeds higher than 12.22 m/s and hence increase the study range of the wind speed values. Moreover, it may be useful to extend the design to a wind farm that consists of multiple wind turbines

connected together. Finally, optimal controllers based on Linear-Quadratic Regulator (LQR) can be used to further enhance the system response.

# References

- [1] F. Bianchi, H. De Battista and R. Mantz, Wind turbine control systems. London: Springer, 2010.
- [2] L. Wang, C. Singh and A. Kusiak, Wind Power Systems. Berlin: Springer Berlin, 2013.
- [3] D. Spera, Wind turbine technology. New York: ASME Press, 2009.
- [4] M. El-Sharkawi, Wind energy. Taylor & Francis Group, 2016.
- [5] D. Wood, Small wind turbines. Springer, 2011.
- [6] "Wind Power Capacity reaches 539 GW, 52,6 GW added in 2017", World wind energy association, 2018. [Online]. Available: <https://wwindea.org/blog/2018/02/12/2017-statistics/>. [Accessed: 27-Dec- 2018].
- [7] Boden, T.A., G. Marland, and R.J. Andres. 2017. Global, Regional, and National Fossil-Fuel CO2 Emissions. Carbon Dioxide Information Analysis Center, Oak Ridge National Laboratory, U.S. Department of Energy, Oak Ridge, Tenn., U.S.A. Available: [https://cdiac.ess-dive.lbl.gov/trends/emis/glo\\_2014.html](https://cdiac.ess-dive.lbl.gov/trends/emis/glo_2014.html). [Accessed: 27- Dec- 2018].
- [8] Wright, Alan D., "Wind Turbine Control Systems," Wind Turbine Technology: Fundamental Concepts in Wind Turbine Engineering, Second Edition, David A. Spera, ASME, New York, 2009.
- [9] A. Kalmikov and K. Dykes, Wind Power Fundamentals. Elsevier Inc., 2010.
- [10] Walker, J. and Jenkins, N., Wind Energy Technology. John Wiley & Sons, Chichester, UK, 1997.
- [11] Panofsky, H., The atmospheric boundary layer below 150 metres. Annual Review of Fluid Mechanics 6, 147–177, 1974.
- [12] Freris, L., editor, Wind Energy Conversion Systems. Prentice Hall, Hertfordshire, UK, 1990.
- [13] Leithead, W., de la Salle, S., and Reardon, D., Role and objectives of control for wind turbines. *IEE Proceedings-C* **138**(2), 135–148, 1991.
- [14] Kaimal, J., Wyngaard, J., Izumi, Y., and Coté, O., Spectral characteristics of surface layer turbulence. *Quarterly Journal of Royal Meteorology Society* **98**, 563–598, 1972.
- [15] Ackermann, T. and Söder, L., An overview of wind energy-status 2002. Renewable and Sustainable Energy Reviews 6(1-2), 67–127, 2002.
- [16] Gardner, P., Garrad, A., Jamieson, P., Snodin, H., and Tindal, A., Wind energy. The facts. Technical report, European Wind Energy Association (EWEA), Brussels, Belgium, 2003.
- [17] M. Hansen, Aerodynamics of wind turbines, 2nd ed. Earthscan, 2008.

- [18] Burton, T., Sharpe, D., Jenkins, N., and Bossanyi, E., *Wind Energy Handbook*. John Wiley & Sons, Ltd., Chichester, UK, 2001.
- [19] Freris, L., editor, *Wind Energy Conversion Systems*. Prentice Hall, Hertfordshire, UK, 1990.
- [20] Durrant, Dale R. "Downslope winds." *Encyclopedia of Atmospheric Sciences*, 644-650, 2003.
- [21] A. Wright, *Modern Control Design for Flexible Wind Turbines*. Washington, D.C: United States. Dept. of Energy, 2004.
- [22] L. Wang et al. (Eds): *Wind Power Systems*, Green Energy and Technology, pp. 407–437. Springer-Verlag Berlin Heidelberg, 2010.
- [23] H. Ibrahim, M. Ghandour, M. Dimitrova, A. Ilinca and J. Perron, "Integration of Wind Energy into Electricity Systems: Technical Challenges and Actual Solutions", *Energy Procedia*, vol. 6, pp. 815-824, 2011.
- [24] Ahmed G. Abo-Khalil, *Impacts of Wind Farms on Power System Stability*. INTECH Open Access Publisher, 2013.
- [25] M. Tandjaoui, C. Benachaiba, O. Abdelkhalek, B. Dennai and Y. Mouloudi, "The Impact of Wind Power Implantation in Transmission Systems", *Energy Procedia*, vol. 36, pp. 260-267, 2013.
- [26] A. Hansen, N. Cutululis, P. Sørensen and F. Iov, "Grid integration impacts on wind turbine design and development", in *IEEE Bucharest Power Tech. Conference*, Bucharest, Romania, 2009.
- [27] M. Cavazzutti, "Fuzzy gain scheduling," Control Engineering Laboratory, Helsinki University of Technology, Sci Rep. 62, 2000
- [28] Ertugal Cam, Ilhan Kocaarslan. Load Frequency Control in Two Area Power Systems Using Fuzzy Logic Controller. Kirikkale University. Turkey. 2004.
- [29] Atul Ikhe, Anant Kulkarni. Dr. Veeresh. Load Frequency Control Using Fuzzy Logic Controller of Two Area thermal-thermal Power System. International Journal of Emerging Technology and Advanced Engineering. 2012.
- [30] K. Tomsovic, "Fuzzy systems applications to power systems", short course Proc. of international conference on intelligent system application to power systems. Brazil Rio de Janeiro, pp. 1-13, 1999.
- [31] K.M. Passino, S. Yurkovich, *Fuzzy Control*, California: Addison-Wesley, 1998.
- [32] N. Naghshineh and A. Ismail, "Advanced Optimization of Single Area Power Generation System Using Adaptive Fuzzy Logic and PI Control," International Research Journal of Engineering and Technology (IRJET), vol. 04, issue: 08, August 2017.

- [33] A. Abo-Khalil, A. Alghamdi, I. Tlili and A. Eltamaly, "Current Controller Design for DFIG-based Wind Turbines Using State Feedback Control", *IET Renewable Power Generation*, 2019.
- [34] Hu, J. Nian, H. Xu and Y. He, "Dynamic Modeling and Improved Control of DFIG Under Distorted Grid Voltage Conditions", *IEEE Transactions on Energy Conversion*, vol. 26, no. 1, pp. 163-175, 2011.
- [35] Y. Zhang and J. Jiao, "Model Predictive Rotor Current Control for Doubly Fed Induction Generators under Unbalanced Grid Voltages," *2018 IEEE International Power Electronics and Application Conference and Exposition (PEAC)*, Shenzhen, pp. 1-5, 2018.
- [36] B. Hamane, M. L. Doumbia, M. Bouhamida and M. Benghanem, "Control of wind turbine based on DFIG using Fuzzy-PI and Sliding Mode controllers," *2014 Ninth International Conference on Ecological Vehicles and Renewable Energies (EVER)*, Monte-Carlo, 2014, pp. 1-8.
- [37] B. Hamane, M. Benghanemm, A. Bouzid, A. Belabbes, M. Bouhamida and A. Draou, "Control for Variable Speed Wind Turbine Driving a Doubly Fed Induction Generator using Fuzzy-PI Control", *Energy Procedia*, vol. 18, pp. 476-485, 2012.
- [38] Yao Xing-jia, Liu Zhong-liang and Cui Guo-sheng, "Decoupling control of Doubly-Fed Induction Generator based on Fuzzy-PI controller," *2010 International Conference on Mechanical and Electrical Technology*, Singapore, pp. 226-230, 2010.
- [39] A. Hansen, P. Sørensen, F. Blaabjerg and J. Becho, "Dynamic Modelling of Wind Farm Grid Interaction", *Wind Engineering*, vol. 26, no. 4, pp. 191-210, 2002.
- [40] R. Ibrahim and S. Watson, "Wind turbine simulation model for the study of combined mechanical and electrical faults", *European Wind Energy Association Annual Event*, Paris, France, 2015.
- [41] A. Junyent-Ferré, O. Gomis-Bellmunt, A. Sumper, M. Sala, and M. Mata, "Modeling and control of the doubly fed induction generator wind turbine", *Simulation Modelling Practice and Theory*, Volume 18, Issue 9, pp. 1365-1381, 2010.
- [42] H. Abu-Rub, *Power electronics for renewable energy systems, transportation, and industrial applications*. Chichester: Wiley, 2014.

- [43] G. Abad, J. Lopez, M. Rodriguez, L. Marroyo and G. Iwanski, *Doubly fed induction machine*. Piscataway: IEEE Press, 2011.
- [44] M. Alberdi, M. Amundarain, A. Garrido and I. Garrido, "Neural control for voltage dips ride-through of oscillating water column-based wave energy converter equipped with doubly-fed induction generator", *Renewable Energy*, vol. 48, pp. 16-26, 2012.
- [45] W. Lin and C. Hong, "A New Elman Neural Network-Based Control Algorithm for Adjustable-Pitch Variable-Speed Wind-Energy Conversion Systems", *IEEE Transactions on Power Electronics*, vol. 26, no. 2, pp. 473-481, 2011.
- [46] Cortajarena and J. De Marcos, "Neural Network Model Reference Adaptive System Speed Estimation for Sensorless Control of a Doubly Fed Induction Generator", *Electric Power Components and Systems*, vol. 41, no. 12, pp. 1146-1158, 2013.
- [47] X. Kong, K. Lee and X. Liu, "Data-driven modelling of a doubly fed induction generator wind turbine system based on neural networks", *IET Renewable Power Generation*, vol. 8, no. 8, pp. 849-857, 2014.
- [48] Y. Tang, H. He, Z. Ni, J. Wen and X. Sui, "Reactive power control of grid-connected wind farm based on adaptive dynamic programming", *Neurocomputing*, vol. 125, pp. 125-133, 2014.
- [49] A. Medjber, A. Guessoum, H. Belmili and A. Mellit, "New neural network and fuzzy logic controllers to monitor maximum power for wind energy conversion system", *Energy*, vol. 106, pp. 137-146, 2016.
- [50] O. Soares, H. Gonçalves, A. Martins and A. Carvalho, "Nonlinear control of the doubly-fed induction generator in wind power systems", *Renewable Energy*, vol. 35, no. 8, pp. 1662-1670, 2010.
- [51] Kh. Belgacem, A. Mezouar and A. Massoum, "Fuzzy Logic Control of Double-Fed induction Generator Wind Turbine," *International Review on Modelling and Simulations (I.R.E.M.O.S.)*, June 2008.

# Appendix - I

## Code 1: PI regulator

```
close all
clear all
clc
%% DFIG parameters -> Rotor parameters referred to the stator side
f=50;
Ps=2e6;
n=1500;
Is=1760;
Vs=690;
Tem=12732;
p=2;
u=1/3;
Vr=2070;
smax=1/3;
Vr_stator=(Vr*smax)*u;
Rs=2.6e-3;
Lsi=0.087e-3;
Lm=2.5e-3;
Rr=2.9e-3;
Ls=Lm+Lsi;
Lr=Lm+Lsi;
Vbus=Vr_stator*sqrt(2);
sigma =1-Lm^2/(Ls*Lr);
Fs=Vs*sqrt(2/3)/(2*pi*f);
J=127;
D=1e-3;
fsw=4e3;
Ts=1/fsw/50;
N=100;
tau_i=(sigma*Lr)/Rr;
tau_n=0.05/4;
wni=100*(1/tau_i);
wnn=1/tau_n;
kp_id=(2*wni*sigma*Lr)-Rr;
kp_iq=kp_id;
ki_id=(wni^2)*Lr*sigma;
ki_iq=ki_id;
kp_n=(2*wnn*J)/p;
ki_n=((wnn^2)*J)/p;
```



## Code 2: Steady State Analysis

```
close all
clear all
clc
%% DFIG parameters -> Rotor parameters referred to the stator side
f=50;
Ps=2e6;
n=1500;
Is=1760;
Vs=690;
Tem=12732;
p=2;
u=1/3;
Vr=2070;
smax=1/3;
Vr_stator=(Vr*smax)*u;
Rs=2.6e-3;
Lsi=0.087e-3;
Lm=2.5e-3;
Rr=2.9e-3;
Ls=Lm+Lsi;
Lr=Lm+Lsi;
Vbus=Vr_stator*sqrt(2);
sigma =1-Lm^2/(Ls*Lr);
Vs=690*sqrt(2/3);
ws=f*2*pi;
%Max and min speed de 2.4MW
wt_nom=18;
wt_min=9;
%Gearbox
N=100;
%torque and speed arrays (Inputs)
wt=[0.9425, 0.9425, 0.9425, 0.9524, 1.0476, 1.1429, 1.2381, 1.3333, 1.4286, 1.5238,
1.6190, 1.7143,1.8095, 1.8850, 1.8850, 1.8850, 1.8850];
Torque=-1e6*[0.0501,0.1164,0.1925,0.2696,
0.3262,0.3883,0.4557,0.5285,0.6067,0.6902,0.7792,0.8736,0.9733,1.0894,1.2474,1.27
45,1.2745,1.2745,1.2745,1.2745];
Temm=Torque/N;
wmm=wt*(60/2/pi)*N;
sss=(1500-wmm)/1500;
%%%%%%%%%% Qs=0 %%%%%%%%%%%
Ref_Qs_=0*ones(size(sss));
i=0;
for ss=sss,
    i=i+1;

    Tem=Temm(i);
    Ref_Qs=Ref_Qs_(i);

    Wm=ws*(1-ss);
    s(i)=ss;

    A=ws*ws*Lm*Lm;
    B=4*Rs*Tem*ws/3-((Vs)^2);
```

```

C=4*Rs*Rs/(9*Lm*Lm)*((Ref_Qs^2)/(ws^2)+(Tem.^2)/(p^2));
X1=(-B+sqrt(B.^2-4*A.*C))./(2*A);
X2=(-B-sqrt(B.^2-4*A.*C))./(2*A);
Fs=Lm*sqrt(X1);
Fs_(i)=Fs;

%Stator Currents
ids=2*Ref_Qs./(3*ws*Fs);
iqs=2*Tem./(3*p*Fs);
Is(i)=sqrt(ids^2+iqs^2);

%Stator Voltages
uds=Rs*ids;
uqs=Rs*iqs+ws*Fs;
Us(i)=sqrt(uds^2+uqs^2);

%Stator Power
Ps(i)=1.5*(Rs*ids.^2+Rs*iqs.^2+ws*Fs.*iqs);
Qs(i)=Ref_Qs;
Mod_Ss=sqrt(Ps.^2+Qs.^2);

%Rotor currents
idr=-Ls*ids/Lm+Fs/Lm;
iqr=-Ls*iqs/Lm;
Ir(i)=sqrt(idr^2+iqr^2);

%wr
wr=ws*ss;

%Rotor voltage
udr=Rr*idr-Lr*wr.*iqr-Lm*wr.*iqs;
uqr=Rr*iqr+Lr*wr.*idr+Lm*wr.*ids;
Vr(i)=sqrt(udr^2+uqr^2);

%Rotor power
Pr(i)=1.5*(udr.*idr+uqr.*iqr);
Qr(i)=1.5*(uqr.*idr-udr.*iqr);
Mod_Sr=sqrt(Pr.^2+Qr.^2);

%Stator flux
Fsd=Ls*ids+Lm*idr;
Fsq=Ls*iqs+Lm*iqr;
Fs_(i)=sqrt(Fsd*Fsd+Fsq*Fsq);

%Rotor flux
Frd=Lr*idr+Lm*ids;
Frq=Lr*iqr+Lm*iqs;
Fr(i)=sqrt(Frd*Frd+Frq*Frq);

%Mechanical power
Pmec(i)=Tem*Wm/p;

%Effeciency

```

```

if Pmec(i) >= 0
    R(i) = Pmec(i) / (Ps(i) + Pr(i));
else
    R(i) = (Ps(i) + Pr(i)) / Pmec(i);
end

end

i=0;
for ss=sss,
    i=i+1;

    Tem=Temm(i);

    Wm=ws*(1-ss);
    s(i)=ss;

    A=ws*ws*Lm*Lm + (Rs*Lm/Ls)^2;
    B=4*Rs*Tem*ws/3/p - (Vs)^2;
    C=4*Rs*Rs*Tem*Tem/(9*p*p*Lm*Lm);
    X1=(-B+sqrt(B.^2-4*A.*C))./(2*A);
    X2=(-B-sqrt(B.^2-4*A.*C))./(2*A);
    ims=sqrt(X1);
    ims_(i)=ims;
    Fs=ims*Lm;

    %Rotor currents
    idr=0;
    iqr=-2*Tem*Ts./(3*p*Lm*Fs);
    Ir(i)=sqrt(idr^2+iqr^2);

    %Stator Currents
    ids=Fs/Ls;
    iqs=-iqr*Lm/Ls;
    Is(i)=sqrt(ids^2+iqs^2);

    %Stator Voltages
    uds=Rs*ids;
    uqs=Rs*iqs+ws*Fs;
    Us(i)=sqrt(uds^2+uqs^2);

    %Stator Power
    Ps(i)=1.5*(Rs*ids.^2+Rs*iqs.^2+ws*Fs.*iqs);
    Qs(i)=1.5*(uqs.*ids-uds.*iqs);
    Mod_Ss=sqrt(Ps.^2+Qs.^2);

    %wr
    wr=ws*ss;

    %Rotor voltage
    udr=Rr*idr-Lr*wr.*iqr-Lm*wr.*iqs;
    uqr=Rr*iqr+Lr*wr.*idr+Lm*wr.*ids;
    Vr(i)=sqrt(udr^2+uqr^2);

```

```

%Rotor power
Pr(i)=1.5*(udr.*idr+uqr.*iqr);
Qr(i)=1.5*(uqr.*idr-udr.*iqr);
Mod_Sr=sqrt(Pr.^2+Qr.^2);

%Stator flux
Fsd=Ls*ids+Lm*idr;
Fsq=Ls*iqs+Lm*iqr;
Fs_(i)=sqrt(Fsd*Fsd+Fsq*Fsq);

%Rotor flux
Frd=Lr*idr+Lm*ids;
Frq=Lr*iqr+Lm*iqs;
Fr(i)=sqrt(Frd*Frd+Frq*Frq);

%Mechanical power
Pmec(i)=Tem*Wm/p;

%Effeciency
if Pmec(i)>=0
    R(i)=Pmec(i)/(Ps(i)+Pr(i));
else
    R(i)=(Ps(i)+Pr(i))/Pmec(i);
end
end

figure(1)

subplot(3,3,1)
hold on
plot(wmm, Temm, 'g', wmm, Temm, 'og', 'linewidth', 1.5);
xlabel('n (rpm)', 'fontsize', 14);
ylabel('Tem (N.m)', 'fontsize', 14);
grid
xlim([700 2000]);

subplot(3,3,2)
% title('Red: Qs=0, Green: idr=0', 'fontsize', 12)
hold on
plot(wmm, Ps+Pr, 'g', wmm, Ps+Pr, 'og', 'linewidth', 1.5);
xlabel('n (rpm)', 'fontsize', 14);

ylabel('Pt (W)', 'fontsize', 14);
grid
xlim([700 2000]);

subplot(3,3,3)
hold on
plot(wmm, Pr, 'g', wmm, Pr, 'og', 'linewidth', 1.5);
xlabel('n (rpm)', 'fontsize', 14);
ylabel('Pr (W)', 'fontsize', 14);
xlim([700 2000]);

subplot(3,3,3)

```

```

hold on
plot(wmm,Ps,'g',wmm,Ps,'*g','linewidth',1.5);
xlabel('n (rpm)','fontsize',14);
ylabel('Ps& Pr (W)','fontsize',14);
grid
xlim([700 2000]);

subplot(3,3,4)
hold on
plot(wmm,Is,'g',wmm,Is,'og','linewidth',1.5);
xlabel('n (rpm)','fontsize',14);
ylabel('Is (A)','fontsize',14);
grid
xlim([700 2000]);

subplot(3,3,5)
hold on
plot(wmm,Ir,'g',wmm,Ir,'og','linewidth',1.5);
xlabel('n (rpm)','fontsize',14);
ylabel('Ir (A)','fontsize',14);
grid
xlim([700 2000]);

subplot(3,3,6)
hold on
plot(wmm,Vr,'g',wmm,Vr,'og',wmm,Us,'g',wmm,Us,'og','linewidth',1.5);
xlabel('n (rpm)','fontsize',14);
ylabel('Vr & Vs (V)','fontsize',14);
grid
xlim([700 2000]);

subplot(3,3,7)
hold on
plot(wmm,Qs,'g',wmm,Qs,'og','linewidth',1.5);
xlabel('n (rpm)','fontsize',14);
ylabel('Qs (VAR)','fontsize',14);
grid
xlim([700 2000]);

subplot(3,3,8)
hold on
plot(wmm,Qr,'g',wmm,Qr,'og','linewidth',1.5);
xlabel('n (rpm)','fontsize',14);
ylabel('Qr (VAR)','fontsize',14);
grid
xlim([700 2000]);

subplot(3,3,9)
hold on
plot(wmm,R,'g',wmm,R,'og','linewidth',1.5);
xlabel('n (rpm)','fontsize',14);
ylabel('Effeciency (pu)','fontsize',14);
grid
xlim([700 2000]);

```

### Code 3: Fuzzy and Fuzzy-PI code

```
close all
clear all
clc

%% DFIG parameters -> Rotor parameters referred to the stator side
% open('Idr_Fuzz.fsi')
curr=struct;
f=50; %stator frequency
Ps=2e6; %rated stator power
n=1500; %rated rotational synchronous speed rpm
Is=1760; %rated stator current
Vs=690; %page 179
Tem=12732; %rated torque
p=2; %pole pairs
u=1/3; %stator/rotor turns ratio
Vr=2070; %rated rotor voltage (not reached)
smax=1/3; %max slip
Vr_stator=(Vr*smax)*u; %rated rotor voltage
Rs=2.6e-3; %stator resistance
Lsi=0.087e-3; %leakage inductance (stator and rotor)
Lm=2.5e-3; %magnitizing inductance
Rr=2.9e-3; %rotor resistance
Ls=Lm+Lsi; %stator inductance
Lr=Lm+Lsi; %rotor inductance
Vbus=Vr_stator*sqrt(2); %DC bus voltage
sigma =1-Lm^2/(Ls*Lr);
Fs=Vs*sqrt(2/3)/(2*pi*f); %stator flux

Vs=690*sqrt(2/3);
ws=f*2*pi;
%%%%%%%%%%%%%%%%%%%%%%%%%%%%%%%%%%%%%%%%%%%%%%%%%%%%%%%%%%%%%%%%%%%%%%%%

J=127/2; %inertia
D=1e-3; %damping
fsw=4e3; %switching freq
Ts=1/fsw/50;%sampling time
%PI regulators

tau_i=(sigma*Lr)/Rr;
tau_n=0.05/4;
wni=100*(1/tau_i);
wnn=1/tau_n;
%kp=199*Rr
kp_id=(2*wni*sigma*Lr)-Rr;

kp_iq=kp_id;
%ki=((100*(Rr/sigma*Lr))^2)*Lr*sigma
ki_id=(wni^2)*Lr*sigma;
ki_iq=ki_id;
kp_n=(2*wnn*J)/p;
ki_n=((wnn^2)*J)/p;

% %Three blade wind model
```

```

N=100;           %Gearbox ratio
Radio=42;       %Radius of the turbine rotor (length of the blade) (m)
ro=1.225;      % air density

% Cp and Ct curves
beta=0;        %pitch angle
ind2=1;

for lambda = 0.1:0.01:11.8    %lambda is the tip speed ratio

    lambdai(ind2)=(1./((1./(lambda-0.02.*beta)+(0.003./(beta^3+1))))); %k1=1 k2=
    Cp(ind2)=0.773.*(151./lambdai(ind2)-0.58.*beta-0.002.*beta^2.14-13.2).*(exp(-
18.4./lambdai(ind2)));
    Ct(ind2)=Cp(ind2)/lambda;
    ind2=ind2+1;
end
tab_lambda=[0.1:0.01:11.8];

% Kopt for MPPT

Cp_max=0.44;
lambda_opt=7.2;
Kopt=((0.5*ro*pi*(Radio^5)*Cp_max)/(lambda_opt^3));

%Power curve in function of wind speed

P=1.0e+06*[0,0,0,0,0,0,0,0.0472,0.1097,0.1815,0.2568,0.3418,0.4437,0.5642,0.7046,
0.8667,1.0518,1.2616,1.4976,1.7613,2.0534,2.3513,2.4024,2.4024,2.4024,2.4024,2.40
24,2.4024];

V=[0.0000,0.5556,1.1111,1.6667,2.2222,2.7778,3.3333,3.8889,4.4444,5.0000,5.5556,6
.1111,6.6667,7.2222,7.7778,8.3333,8.8889,9.4444,10.0000,10.5556,11.1111,11.6667,1
2.2222,12.7778,13.3333,13.8889,14.4444,15.0000];

figure
subplot(1,2,1)
plot(tab_lambda,Cp,'linewidth',1.5)

xlabel('lambda','fontsize',14)
ylabel('Cp','fontsize',14)
subplot(1,2,2)
plot(V,P,'linewidth',1.5)
grid
xlabel('Wind Speed (m/s)','fontsize',14)
ylabel('Power (W)','fontsize',14)

Idr_Fuzz5= readfis('Idr_Fuzz5')

```